Economic Geology, v. 100, pp. 887–904

Regional Geochemistry of Tertiary Igneous Rocks in Central Chile: Implications for the Geodynamic Environment of Giant Porphyry Copper and Epithermal Gold Mineralization

PETER HOLLINGS,[†,*] DAVID COOKE,

Centre for Ore Deposit Research, University of Tasmania, Private Bag 79, Hobart, Tasmania, Australia 7001

AND ALAN CLARK

Department of Geological Sciences and Geological Engineering, Miller Hall, Queen's University, Kingston, Ontario, Canada K7L 3N6

Abstract

The giant porphyry copper-molybdenum deposits of central Chile formed within a thick sequence of Cretaceous to Pliocene volcanic rocks. The predominantly calc-alkaline basaltic andesites of the Cretaceous Las Chilcas Formation are characterized by La/Sm_n ratios of 1.8 to 2.5 and Sm/Yb_n of 1.8 to 2.8. The upper Oligocene to lower Miocene Abanico Formation (variously defined as the Los Pelambres, Abanico, or Coya Machalí Formations) ranges from basalt to rhyolite in composition and exhibits a broad southward transition from calc-alkaline to tholeiitic. All samples from this formation are characterized by LREE enrichment and moderately, or locally strongly, fractionated HREE (La/Sm_n = 1.3–4.1; Sm/Yb_n = 1.5–5.8). The basaltic andesites and andesites of the middle Miocene Salamanca Formation have REE chemistry similar to that of the Upper Cretaceous strata (La/Sm_n = 1.5–2.7; Sm/Yb_n = 1.6–2.7). The overlying middle Miocene Farellones Formation ranges from tholeiitic to calc-alkaline and from basalt to andesitic and has a similar LREE enrichment and fractionated HREE (La/Sm_n = 1.7–2.5; Sm/Yb_n = 1.7–3.3). The Pliocene La Copa Rhyolite Complex, however, is strongly LREE enriched and HREE depleted (La/Sm_n = 3.8–3.9; Sm/Yb_n = 4.2–4.7). Overall, the trace element geochemistry of the Cretaceous to middle Miocene volcanic rocks is characterized by enriched LREE and negative Nb anomalies, consistent with an arc setting, with only minor differences in the abundance of most elements. Crustal thickening during the Miocene in central Chile has been suggested to have been responsible for a transition from an amphibole- to garnet-dominated residual mineralogy resulting in the release of fluids that enabled the formation of giant copper porphyry deposits. However, the gradual increase in La/Yb through the early, middle, and late Miocene reported in earlier studies and interpreted to be a response to crustal thickening is not observed in the regional data. Instead, a rapid change in the geochemical signature between the end of the eruption of the Farellones Formation and the eruption of the high La/Yb La Copa Rhyolite Complex implies a more abrupt change in the tectonic environment. Isotopic data broadly support this, although lower ε_{Nd} values in the Farellones Formation imply a greater role for crustal contamination in younger suites. In the absence of gradual crustal thickening, it is suggested that the subduction of the Juan Fernández Ridge may have been the key geodynamic process responsible for the genesis of the three middle Miocene to lower Pliocene giant porphyry copper deposits in central Chile, possibly by promoting crustal-scale faulting and even acting as a source of metals.

Introduction

THE CA. 500-km-long segment of the central Andean orogen between latitudes 27° and 34° south hosts an exceptional number of world-class magmatic-hydrothermal centers (Fig. 1). These include three of the largest known porphyry copper-molybdenum deposits (El Teniente: 75 Mt Cu; Río Blanco-Los Bronces: 49 Mt Cu; Los Pelambres-El Pachón: 21 Mt Cu; Cooke et al., 2005) as well as the unusually high grade El Indio high- to low-sulfidation epithermal vein swarm (4.506 Moz Au), the Pascua-Lama and Veladero high-sulfidation deposits, with an aggregate resource of 34.2 Moz Au, the cluster of high-sulfidation Au-Ag, porphyry Cu-Au, and porphyry Au centers of the Maricunga district, and, far to the east in Argentina, the Au-rich porphyry systems of the Farallón Negro volcanic complex and its outliers (Harris et al., 2005). All of these are of Neogene age, and the great majority were emplaced during the middle Miocene to early Pliocene (i.e., between ca. 12 and ca. 4.5 Ma). Much of this segment of the South American plate boundary has experienced subhorizontal subduction of oceanic lithosphere (Cahill and Isacks, 1992) since the late middle Miocene (e.g., Kay et al., 1991, 1999; Kay and Abruzzi, 1996; Yañez et al., 2001), and the ore deposits are located either in the center of the "flat slab" (the El Indio-Pascua belt) or adjacent to its gradational northern (Maricunga, Farallón Negro) and abrupt southern (Los Pelambres to El Teniente) boundaries (Fig. 1). The temporal and spatial conjunction of slab flattening with outsize and exceptionally metal rich hydrothermal activity has prompted metallogenic modeling directly linking large-scale geodynamic processes with Cu and Au mineralization. Skewes and Stern (1994, 1995, 1996), Kay and Mpodozis (2001, 2002), and Kay et al. (2005) have addressed the tectonic and geochemical environment of the giant Miocene to Pliocene porphyry Cu-Mo deposits, and Kay et al. (1994) have documented the relationships between the chemistry of the arc volcanic rocks and Au-rich mineralization in the wider

[†] Corresponding author: e-mail, peter.hollings@lakeheadu.ca

[*] Current address: Department of Geology, Lakehead University, 955 Oliver Road, Thunder Bay, Ontario, Canada P7B 5E1.

0361-0128/05/3527/887-18 $6.00

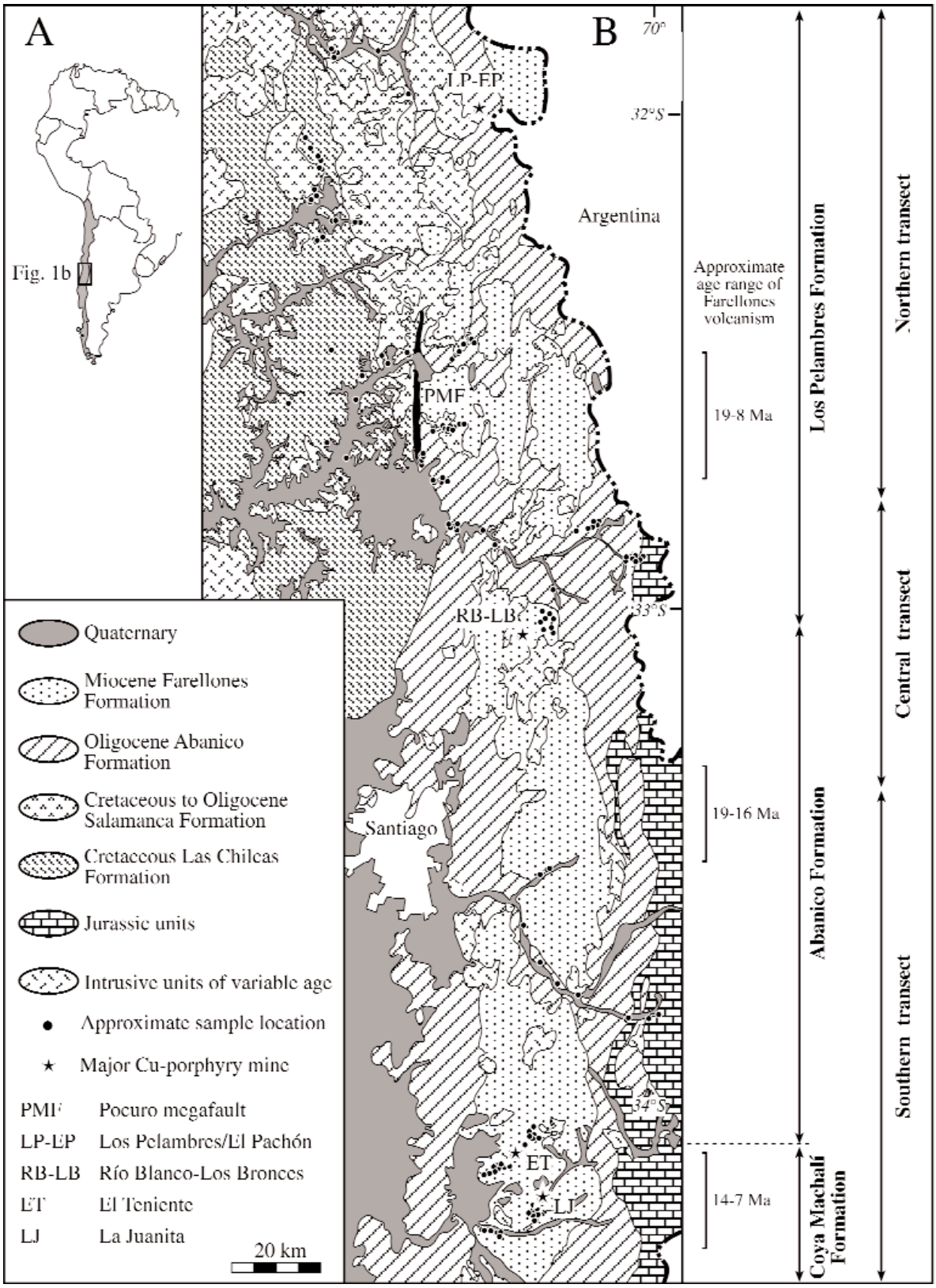

FIG. 1. Simplified geologic map of central Chile, showing approximate locations of the 88 representative samples analyzed in this study and major Cu porphyry deposits. Right-hand column illustrates the approximate extent of the traditional terminology applied to the Oligocene volcanic rocks of central Chile, referred to as the Abanico Formation herein (see text for discussion). Age data in right-hand column from Vergara et al. (1988). Map modified after Rivano et al. (1993), Rivano and Sepulveda (1986), and Thiele (1979).

Maricunga-Farallón Negro transect (cf. Sasso and Clark, 1998). Comprehensive metallogenic models incorporating porphyry Cu-Mo and epithermal Au-Ag (-Cu) deposits have been proposed by Kay et al. (1999) and Kay and Mpodozis (2001), who argued that identical geodynamic and petrogenetic processes were favorable for both. They proposed that progressive slab flattening through the Miocene caused radical thickening of the sub-arc continental crust and a concomitant depression of the major locus of crustal anatexis. Specifically, rare earth element data were interpreted as evidence for a transition in residual mineralogy from clinopyroxene, through amphibole to garnet, and the onset of fertile hydrothermal activity was ascribed to large-scale breakdown of hornblende in the deep crust, probably abetted by widespread dewatering at shallower levels. In contrast, Skewes and Stern (1994, 1995, 1996) argued that the tectonic erosion of the leading edge of the South American plate (Stern, 1989, 1991, 2001) and the resulting contamination of the sub-arc mantle were the key factors in modifying the chemistry of the arc volcanic rocks and promoting fertile hydrothermal activity.

Both of the above interpretations of the Neogene tectonic and magmatic-hydrothermal evolution of this Andean segment acknowledge the possibility that slab flattening may have been caused by the diachronous, north to south, underthrusting of the buoyant Juan Fernández Ridge (Yañez et al., 2001), which would probably have resulted in increased subduction erosion. Kay and Mpodozis (2002), however, argued that much of the widespread magmatism in the flat-slab foreland is unlikely to have resulted from the southward sweep of the subducting ridge, even if this exerted a >200-km north-south "swath of influence" on the overlying mantle and crust. A critical factor in these arguments is the geochronologic database, which is still incomplete for many key areas. The implied correlation between ridge subduction and giant porphyry Cu-Mo formation (e.g., Skewes and Stern, 1995) relies largely on the K-Ar evidence (Quirt et al., 1971) for a southward, Miocene to Pliocene migration of hydrothermal activity from Los Pelambres, through Río Blanco-Los Bronces, to El Teniente. However, new geochronologic data for Río Blanco (Deckart et al., 2005) demonstrate that this magmatic-hydrothermal center formed at broadly the same time as El Teniente ~110 km farther south (Maksaev et al., 2002; Muniziga et al., 2002; Cannell et al., 2003). Similarly, a robust ^{40}Ar-^{39}Ar database for volcanism, hypabyssal intrusion, and hydrothermal activity in the El Indio-Pascua Au belt (Bissig et al., 2001) shows that economic epithermal mineralization began several million years after the transition to high-pressure anatectic melting, thereby divorcing ore formation from the postulated large-scale destruction of amphibole in the deep crust (Bissig et al., 2002; cf. Kay et al., 1999; Kay and Mpodozis, 2001).

Present study

To address some of these questions, we examine an expanded regional geochemical database on Neogene and Upper Cretaceous volcanic and hypabyssal rocks from central Chile. The samples are from latitudes between 32° and 34°15' S and include samples from the Los Pelambres, Río Blanco-Los Bronces, and El Teniente porphyry deposits. Trace element data are provided for fresh and least altered samples, and a representative subset has been analyzed for Sr and Nd isotopes. The regional scale of our data set, collected throughout central Chile from a diverse range of units derived from different volcanic centers over a significant time range, does not permit detailed petrogenetic studies of individual formations. Rather we compare our data set to other more detailed studies of petrogenetic processes and use the data to make inferences about changes in the tectonic setting of central Chile since the Cretaceous. The compositional evolution of the Andean arc is examined in several transects, including at the latitude of the El Indio-Pascua belt (Bissig et al., 2002), which provides evidence of the effects of slab flattening on magma chemistry and the timing relationships between epithermal mineralization and arc evolution. We also compare our new analyses with the most detailed geochemical data set for this region, which formed the basis for the work of S. Kay and A. Kurtz (1995, unpub. report for CODELCO-Chile, 180 p.) and focused on the El Teniente district (Kay et al., 1999, 2005; Kay and Mpodozis, 2001). Finally we reevaluate the potential role of ridge subduction on porphyry development in the light of the new age data for Río Blanco (Deckart et al., 2005), El Teniente (Maksaev et al., 2002; Muniziga et al., 2002; Cannell et al., 2003), and Los Pelambres (Mathur et al., 2001; Bertens et al., 2003). We also contribute to the geochronologic database for the critical middle to upper Miocene igneous rocks of the region with five new ^{40}Ar-^{39}Ar ages for selected volcanic and intrusive units.

Regional Geology

The Cordillera Principal of central Chile between 31°30' and 34°30' S (Fig. 1) exposes both upper Paleozoic basement and Triassic to Recent Andean volcanic, intrusive, and sedimentary rocks, the latter incorporating the northern limit of the Southern Volcanic zone that extends to 46°S. The Southern Volcanic zone is underlain by a relatively steeply dipping (~30°) segment of the Nazca plate, but the dip of the slab decreases to the north as the flat-slab zone is approached. The transition between the Southern Volcanic zone and nonvolcanic flat-slab segment coincides with a kink in the downgoing slab, the offshore projection of which is aligned with the Juan Fernández Ridge (Yañez et al., 2002). Clarification of the geochemical history of the volcanic arc in this region is hindered by a paucity of modern geochronologic data and the difficulty of even local correlation of the fundamentally similar, commonly andesite-dominated volcanic successions. In this section, we review the stratigraphic relationships and clarify some of the inconsistent nomenclature.

The oldest unit investigated herein is the Cretaceous Las Chilcas Formation (Fig. 1), which overlies the Lower Cretaceous Lo Prado and Veta Negra Formations in the northern part of the study area. The Las Chilcas Formation comprises ca. 3,500 m of predominantly subaerial volcanic units characterized by rapid vertical and horizontal facies changes that are marked by recurrent episodes of marine incursion (Rivano, 1995). This is interpreted as evidence for emplacement over relatively thin crust (Rivano, 1995). Andesitic lavas, tuffs, and agglomerates predominate in the lower part of the formation, but sedimentary units, including lahars and mass flow units, are abundant at higher levels (Rivano, 1995). K-Ar ages for the Las Chilcas Formation range from 64 to 125 Ma (Rivano

et al., 1993). This large age range may reflect the incomplete characterization of the formation but more probably results from errors in the age determinations, which were obtained mainly by whole-rock analyses of variably altered specimens.

The continental Abanico Formation, best documented south of the Río Blanco and Los Bronces mines (Fig. 1), comprises relatively unaltered tholeiitic andesitic lavas, breccias, ignimbrites, and tuffaceous sandstones (Charrier et al., 2002; Nyström et al., 2003), inferred to represent a basin infill sequence (Godoy et al., 1999). These rocks have K-Ar ages ranging from 16.1 to 36 Ma (Charrier et al., 2002, and references therein) and are probably equivalent to the Coya Machalí Formation in the vicinity of El Teniente mine (Fig. 1), where K-Ar mineral ages of 20.5 to 27.7 Ma have been reported (S. Kay and A. Kurtz, 1995, unpub. report for CODELCO-Chile, 180 p.), as well as to the Los Pelambres Formation north of 33°S (Rivano, 1995).

The Salamanca Formation was mapped by Rivano et al. (1993) in the vicinity of the Pocuro megafault north of the Río Blanco-Los Bronces deposit (Fig. 1) and is separated from the underlying Abanico Formation by an angular unconformity (Rivano, 1995). It comprises continental andesitic lavas and andesitic to dacitic volcaniclastic rocks with intercalated rhyolite and is estimated to have maximum and average thicknesses of 2,500 and ~1,300 m, respectively (Rivano, 1995). Whole-rock K-Ar ages of the formation to the east of the megafault (Fig. 1) range from 11.4 to 30.1 Ma.

The younger and better defined Farellones Formation (Rivano et al., 1993) is the dominant Miocene arc succession in central Chile and forms a longitudinal belt ~400 km long and 24 to 65 km wide (Fig. 1; Vergara et al., 1988). It unconformably overlies the Salamanca and older formations but is locally conformable with the Abanico Formation (Godoy et al., 1999; Charrier et al., 2002; Nyström et al., 2003). The rocks range from basaltic through dacitic to rhyolitic. Felsic rocks are more abundant in the north (Vergara et al., 1988). Volcanism has been considered to young from north to south (Fig. 1), but most of the published K-Ar mineral ages range from 15 to 18 Ma (Beccar et al., 1986; Vergara et al., 1988). U-Pb zircon ages of 16.77 ± 0.25 (2σ) and 17.20 ± 0.05 Ma for two andesitic units from the immediate Río Blanco mine area (Deckart et al., 2005) confirm that these rocks are middle Miocene in age. In the Teniente district (Fig. 1), S. Kay and A. Kurtz (1995, unpub. report for CODELCO-Chile, 180 p.) followed Godoy (1993) in assigning a succession of volcanic rocks, previously incorporated into the Farellones Formation, to the Teniente Volcanic Complex. This, in turn, is subdivided into the Maqui Chico Group (ca. 12–15.2 Ma) and the Lower and Upper Sewell Groups, the eruption of which extended approximately from 10 to 6 Ma. The argument for crustal thickening of S. Kay and A. Kurtz (1995, unpub. report for CODELCO-Chile, 180 p.) and Kay et al. (2005) rely extensively on geochemical analyses of the Teniente Volcanic Complex, which we infer to overlap temporally with the later stages of eruption of the Farellones Formation.

Compositionally diverse granitoid rocks, grouped as the San Francisco batholith in the Río Blanco-Los Bronces area, intrude the Farellones Formation and older units. These have yielded K-Ar ages from 7.4 to 20.1 Ma (Serrano et al., 1996), and Kurtz et al. (1997) provide similar ^{40}Ar-^{39}Ar (furnace) incremental-heating ages from 5.3 to 19.8 Ma for five plutonic complexes between 33°33' and 35°15' S. U-Pb zircon ages (Deckart et al., 2005) for the granitoid host rocks of the Río Blanco deposit define two intrusive episodes at 11.96 and 8.19 to 8.40 Ma. The latter preceded the initiation of Cu-Mo mineralization at Río Blanco at ca. 6.3 Ma (Deckart et al., 2005). At El Teniente, U-Pb dating of the dacite intrusions indicates emplacement ages of 5.58 to 4.42 Ma, with Re-Os ages of molybdenite indicating that mineralization occurred from 5.60 to 4.42 Ma (Maksaev et al., 2002; Muniziga et al., 2002; Cannell et al., 2003). This contrasts with the molybdenite Re-Os ages of 10.75 to 10.40 Ma (Mathur et al., 2001) and 11.18 to 11.08 Ma (Bertens et al., 2003) from Los Pelambres. The age of the Los Pelambres deposit is also supported by U-Pb zircon ages for the late porphyries of 11.56 to 11.24 Ma and $^{40}Ar/^{39}Ar$ ages of magmatic and hydrothermal minerals associated with the deposit of 12.39 to 10.19 Ma.

The youngest rocks studied herein are those of the Pliocene La Copa rhyolite complex, which crops out as a large body comprising numerous felsic intrusive phases and with an exposed vertical extent of at least 900 m along the boundary between the Río Blanco and Los Bronces deposits (Toro, 1986; Davidson et al., 2005). The La Copa complex was the final intrusion to be emplaced into the ore deposit and has been dated at 3.9 to 4.9 Ma (Serrano et al., 1996, and references therein). The breccias of the dacite chimney that underlie and predate the La Copa rhyolite complex at Río Blanco are strongly seriticized but essentially barren. This dacite has yielded a SHRIMP U-Pb zircon age of 4.92 ± 0.02 Ma (Deckart et al., 2005). Although the La Copa complex is predominantly intrusive, there is evidence for an extrusive phase dominated by rhyolitic tuffs, which are exposed at the top of the vertical section. On the Los Bronces side of the deposit, an ignimbrite of the La Copa complex has been recognized overlying a volcaniclastic mass-flow unit with a soil horizon developed at its upper contact.

Analytical Techniques and Sampling Methodology

A total of 270 samples, predominantly of Cretaceous and younger volcanic rocks, were collected from the study area. Field and petrographic observations were used to select a subset of 88 least altered samples for analysis (Fig. 1). However, in order to provide adequate temporal and spatial coverage, a number of weakly to moderately altered samples were included in the database. Our interpretation of geochemical data focuses on elements that are relatively insensitive to alteration, including Ti, Al, high field strength elements (HFSE), and, particularly, rare earth elements (REE).

X-ray fluorescence analysis of major and some trace elements was performed on 88 samples at the School of Earth Sciences, University of Tasmania, using a Philips PW1480 X-ray spectrometer. Additional trace element and REE analyses were carried out on a subset of 45 samples at the Centre for Ore Deposit Research at the University of Tasmania using an Agilent HP4500 quadrupole ICP-MS and the methodology of Yu et al. (2001). Ten samples were analyzed for radiogenic isotopes at the CSIRO laboratory in North Ryde, and five were analyzed at the University of Adelaide. At CSIRO, Sr was separated on AG50W-X8 cation exchange resin. The REE were collected from this separation and Nd and Sm

then separated further in hexyl di-ethyl hydrogen phosphate (HDEHP)-coated bio-beads. Isotopic compositions were measured on a VG 354 thermal ionization mass spectrometer fitted with seven collectors. Samples were run in dynamic mode with an ion beam intensity of 3×10^{-11} A of ^{88}Sr and 0.5 to 1.0×10^{-11} A of ^{144}Nd. Six blocks of nine $^{87}Sr/^{86}Sr$ ratios were measured for each sample, yielding a total of 54 determinations. $^{87}Sr/^{86}Sr$ ratios were normalized to $^{86}Sr/^{88}Sr = 0.1194$, using an exponential correction law in order to correct for mass fractionation during analysis. For Nd data, eight to ten blocks of nine $^{143}Nd/^{144}Nd$ ratios were measured for each sample, yielding a total of 72 to 90 determinations, normalized to $^{146}Nd/^{144}Nd = 0.7219$, using an exponential correction law in order to correct for mass fractionation during analysis. The raw data were filtered using a 2σ rejection criterion. Measured blanks had a negligible effect on the measured ratios. The precision of individual analyses at 95 percent confidence limits, determined as two standard errors of the mean, was typically between 0.0010 and 0.0020 percent (internal precision). Measurements of the SRM987 standard during the period of analysis yielded a $^{87}Sr/^{86}Sr$ ratio of 0.710250 ± 16 ($n = 33$) and the O'Nions standard yielded a $^{143}Nd/^{144}Nd$ ratio of 0.511118 ± 10 ($n = 6$).

Five samples were selected for ^{40}Ar-^{39}Ar dating at Queen's University, using an 8-W Lexel 3500 continuous argon-ion laser for step-heating and total fusion. Blanks, measured routinely, were subtracted from the sample gas fractions. The extraction blanks were typically $<10 \times 10^{-13}$, $<0.5 \times 10^{-13}$, $<0.5 \times 10^{-13}$, and $<0.5 \times 10^{-13}$ cm^{-3} STP for masses 40, 39, 37, and 36, respectively. Measured argon-isotope peak heights were extrapolated to zero time, normalized to the $^{40}Ar/^{39}Ar$ atmospheric ratio (295.5) using measured values of atmospheric argon and corrected for neutron-induced ^{40}Ar from potassium, ^{39}Ar and ^{36}Ar from calcium using the production ratios of Onstott and Peacock (1987), and ^{36}Ar from chlorine (Roddick, 1983). Ages and errors were calculated using formulas given by Dalrymple et al. (1981) and the constants recommended by Steiger and Jaeger (1977). Isotope correlation analysis used the formulas and error propagation of Hall (1981) and the regression of York (1969). Errors shown on the age spectra represent the analytical precision at 2σ, assuming that the errors in the ages of the flux monitors are zero. The ages and J values for the intralaboratory standard MAC-83 biotite at 24.36 Ma are referenced to TCR sanidine at 28.0 Ma (Baksi et al., 1996).

Results

Representative whole-rock geochemical analyses and isotope data for samples from central Chile are presented in Table 1. The full data set is available from the senior author upon request.

Whole-rock geochemistry

Samples from the Las Chilcas Formation are predominantly basaltic andesite but range from basalt to dacite (SiO_2 = 51–66 wt %; Table 1). The samples are calc-alkaline (Fig. 2) and include medium and high K members. They are LREE enriched (La/Sm_n = 1.8–2.5) with moderately fractionated HREE (Sm/Yb_n = 1.8–2.8) and negative Nb anomalies typical of magmas formed above a subduction zone (Fig. 3).

TABLE 1. Whole-Rock Geochemistry and Isotopic Data for Representative Volcanic Rocks from Central Chile (all values recalculated to 100% anhydrous)

	Las Chilcas Formation					Salamanca Formation						Abanico Formation									
	CN53	CN59	CN62	CN72	CN111	CN103	CN106	CN69	CN46	CN48	CN82	CA36	CE66	CE68	CE69	CV3	CV7	CN11	CN18	CN20	CA38	CA60
SiO_2 (wt %)	65.56	58.00	53.23	54.32	53.06	56.39	53.51	53.17	53.80	50.76	70.88	55.57	54.13	58.13	55.70	51.03	57.32	56.96	71.10	75.12	52.31	52.25
TiO_2	0.86	0.57	1.05	1.17	0.82	0.74	0.90	0.86	1.04	1.04	0.35	1.01	0.99	1.47	1.15	1.46	1.13	0.91	0.48	0.26	1.08	1.24
Al_2O_3	15.26	19.76	17.73	17.83	17.61	19.03	19.37	18.76	18.58	21.94	14.68	17.29	17.77	15.49	17.13	19.61	17.77	18.94	14.85	13.43	19.51	19.21
Fe_2O_3	7.09	6.38	10.38	9.00	8.70	8.23	8.83	9.88	8.57	9.58	3.17	10.18	9.96	10.08	8.28	10.46	9.57	7.66	3.16	1.67	9.74	9.73
MnO	0.05	0.14	0.24	0.14	0.37	0.19	0.15	0.20	0.13	0.19	0.06	0.19	0.20	0.23	0.11	0.20	0.12	0.12	0.05	0.04	0.22	0.12
MgO	1.24	2.20	3.91	4.14	6.45	3.31	4.12	3.17	4.32	2.31	0.54	3.64	4.01	2.49	4.78	3.02	2.02	3.88	0.96	0.28	3.87	4.74
CaO	0.96	3.66	4.91	8.23	5.82	7.77	8.61	9.78	8.78	10.63	1.32	6.75	8.43	5.90	7.05	9.29	2.27	5.19	5.33	0.77	7.50	3.19
K_2O	5.68	2.46	4.16	1.52	2.43	0.14	1.07	1.01	1.36	0.27	5.43	1.13	1.11	1.51	1.77	1.09	3.84	1.55	0.70	4.56	1.14	3.21
Na_2O	2.77	6.62	3.88	3.30	4.49	3.97	3.21	2.92	3.18	3.12	3.49	4.06	3.20	4.26	3.73	3.48	5.58	4.57	3.31	3.83	4.35	5.85
P_2O_5	0.55	0.21	0.53	0.36	0.24	0.23	0.24	0.26	0.24	0.16	0.09	0.18	0.19	0.42	0.30	0.35	0.38	0.20	0.08	0.05	0.29	0.46
LOI	2.39	2.51	2.71	2.14	3.04	2.78	1.05	3.29	1.82	0.53	1.67	1.70	1.35	0.81	0.34	1.03	2.06	3.50	8.03	0.59	3.63	1.50
Mg#[1]	0.28	0.43	0.45	0.50	0.62	0.47	0.51	0.41	0.53	0.35	0.27	0.44	0.47	0.35	0.56	0.39	0.32	0.53	0.40	0.27	0.47	0.52
Cr (ppm)	1.64	1.74	15.93	42.20	83.02	4.83	18.19	4.03	48.49	7.54	3.76	11.39	17.16	2.40	96.16	5.36	25.83	42.39	15.77	1.61	8.42	14.52
Co	9.46	11.38	23.51	23.44	30.00	19.48	24.83	20.88	28.53	18.87	4.86	27.30	30.90	13.53	27.12	21.86	24.45	18.66	7.29	1.91	28.17	27.97
Ni	1.54	0.82	9.06	26.77	32.67	3.60	14.41	2.02	38.22	4.48	2.24	7.12	6.16	1.19	45.23	3.94	13.38	20.52	6.14	1.20	9.55	17.16
Rb	198	61	164	37	52	3	24	13	29	9	165	20	41	21	61	26	80	26	78	181	16	63
Sr	126	798	557	456	627	456	631	579	532	475	496	353	412	397	525	490	589	369	300	78	724	519
Cs	7.87	6.79	11.37	0.78	3.62	0.94	8.93	0.22	4.13	1.33	1.89	0.66	2.75	0.30	3.15	1.97	1.59	0.51	102.10	3.12	0.72	2.22
Ba	842.5	591.1	815.0	359.0	1203.0	231.5	448.2	322.0	307.6	120.8	609.9	395.4	277.9	365.9	415.3	300.1	1090.6	672.2	648.8	625.6	508.8	930.0

TABLE 1. *(Cont.)*

	Las Chilcas Formation					Salamanca Formation						Abanico Formation										
	CN53	CN59	CN62	CN72	CN111	CN103	CN106	CN69	CN46	CN48	CN82	CA36	CE66	CE68	CE69	CV3	CV7	CN11	CN18	CN20	CA38	CA60
Sc	21.8	10.0	29.2	25.0	30.4	17.3	28.5	20.1	19.9	35.1	9.6	28.0	35.0	34.9	20.7	31.8	18.8	22.8	9.9	3.9	24.5	27.3
V	99.3	76.7	275.0	218.7	269.5	139.8	265.3	192.2	197.1	248.8	60.7	273.2	279.2	97.9	190.0	257.4	129.9	176.7	51.3	9.8	249.1	300.8
Ta	0.77	0.28	0.37	0.45	0.17	0.16	0.23	0.15	0.26	0.11	0.73	0.18	0.21	0.47	0.54	0.62	0.76	0.49	0.93	0.73	0.20	0.44
Nb	10.86	4.10	5.65	5.82	2.37	2.88	3.64	2.59	3.46	1.91	9.15	1.93	3.14	6.65	6.92	9.09	9.50	6.43	9.46	6.64	3.08	6.60
Zr	448.1	110.0	218.4	189.7	130.8	71.7	115.3	91.7	103.3	62.5	378.4	81.6	104.8	166.7	197.6	137.4	201.0	221.1	332.3	189.8	105.9	223.1
Hf	11.68	3.05	6.16	5.36	3.87	2.12	3.41	2.52	3.12	1.85	11.88	2.40	3.09	4.66	5.45	3.70	5.58	6.27	9.62	5.78	3.02	6.20
Th	16.39	2.76	7.96	7.16	4.22	1.54	2.87	1.96	2.35	0.73	24.71	2.85	5.17	3.13	6.72	2.22	6.64	10.56	24.55	23.13	2.17	10.05
U	3.87	0.75	2.34	1.91	1.31	0.34	0.89	0.52	0.80	0.16	6.66	0.75	1.06	0.88	2.01	0.66	1.39	3.00	6.84	6.22	0.56	2.27
Y	44.6	20.6	32.9	26.5	19.7	17.9	21.5	20.7	16.7	22.5	29.0	18.5	20.8	37.2	20.1	25.2	22.4	26.5	31.4	20.9	19.8	34.3
La	44.06	11.28	27.55	18.09	14.65	9.51	13.74	11.17	12.43	7.44	24.00	9.56	12.06	18.55	25.49	15.05	21.85	18.65	37.62	21.02	13.55	32.29
Ce	98.37	28.11	62.09	43.12	35.17	20.26	30.52	28.13	29.18	20.01	54.92	24.11	26.96	45.37	57.19	32.43	50.03	43.22	69.70	45.07	31.41	74.11
Pr	13.24	3.76	8.58	6.17	5.25	3.22	4.24	3.78	3.80	2.42	7.20	2.67	3.25	5.85	7.48	4.44	6.67	5.89	7.20	5.67	4.28	9.12
Nd	55.84	15.59	35.67	25.96	20.63	14.71	19.51	17.68	15.79	12.97	27.76	13.53	15.92	27.22	30.40	20.81	28.39	23.94	29.90	20.32	20.53	41.52
Sm	11.23	4.03	8.34	6.19	5.07	3.74	4.62	4.19	4.17	3.28	5.74	3.17	3.74	6.81	6.55	4.96	6.14	5.47	5.88	3.98	4.77	8.80
Eu	1.85	1.27	1.89	1.44	1.34	1.25	1.34	1.34	1.23	1.24	0.60	1.10	1.14	2.12	1.54	1.61	1.66	1.23	0.78	0.51	1.40	2.08
Gd	9.66	4.04	7.58	5.87	4.72	3.82	4.49	4.17	3.99	3.89	4.98	3.43	4.04	7.08	5.50	5.23	5.68	5.17	5.36	3.47	4.47	7.89
Tb	1.43	0.63	1.08	0.88	0.68	0.57	0.66	0.65	0.64	0.63	0.79	0.60	0.68	1.20	0.79	0.82	0.82	0.79	0.93	0.57	0.71	1.19
Dy	8.24	3.96	6.30	5.13	3.81	3.35	4.04	3.87	3.49	3.86	4.91	3.69	4.12	7.27	4.24	4.89	4.67	4.58	5.41	3.52	4.02	6.63
Ho	1.65	0.82	1.28	1.06	0.77	0.67	0.82	0.79	0.69	0.83	1.06	0.80	0.89	1.57	0.80	1.00	0.90	0.93	1.16	0.75	0.84	1.34
Er	4.73	2.44	3.64	2.96	2.25	1.90	2.38	2.34	1.88	2.39	3.38	2.35	2.51	4.38	2.18	2.91	2.54	2.69	3.45	2.29	2.29	3.67
Yb	4.47	2.49	3.39	2.82	2.03	1.78	2.26	2.20	1.74	2.21	3.66	2.35	2.49	4.27	1.84	2.65	2.35	2.49	3.66	2.50	2.19	3.40
Lu	0.68	0.38	0.51	0.41	0.32	0.27	0.34	0.34	0.26	0.34	0.59	0.34	0.36	0.64	0.27	0.41	0.36	0.38	0.58	0.39	0.33	0.50
La/Yb	9.87	4.53	8.14	6.42	7.22	5.35	6.09	5.07	7.16	3.37	6.57	4.07	4.85	4.35	13.86	5.67	9.30	7.49	10.28	8.41	6.18	9.51
Cu	169.7	70.1	127.8	79.4	223.4	238.6	90.0	82.3	81.0	85.3	32.2	80.7	72.6	9.6	75.0	87.3	103.2	75.4	42.1	19.8	95.4	50.1
Zn	7.4	22.5	39.7	173.2	9.2	217.0	57.9	26.7	108.0	56.9	70.1	55.2	91.2	116.3	89.3	63.8	14.6	60.1	28.2	10.1	111.2	5.9
Mo	1.29	0.84	1.66	1.69	0.75	0.67	1.01	0.67	0.79	0.58	2.83	0.80	1.44	1.22	1.72	0.83	0.84	0.98	4.98	1.11	0.51	0.41
Pb	12.71	3.90	29.19	7.87	4.95	39.08	7.48	5.38	4.43	8.14	7.32	4.88	6.08	4.64	10.94	5.15	4.19	9.85	21.09	8.25	4.52	3.14
La/Yb_n[2]	7.07	3.25	5.83	4.61	5.17	3.84	4.37	3.63	5.13	2.41	4.71	2.92	3.48	3.12	9.93	4.07	6.67	5.37	7.37	6.03	4.43	6.82
La/Sm_n	2.54	1.81	2.13	1.89	1.87	1.64	1.92	1.72	1.92	1.47	2.70	1.95	2.08	1.76	2.51	1.96	2.30	2.20	4.13	3.41	1.84	2.37
Gd/Yb_n	1.79	1.34	1.85	1.72	1.92	1.78	1.65	1.57	1.90	1.46	1.13	1.21	1.34	1.37	2.47	1.63	2.00	1.72	1.21	1.15	1.69	1.92
Sm/Yb_n	2.79	1.80	2.74	2.44	2.78	2.34	2.28	2.11	2.67	1.65	1.74	1.50	1.67	1.77	3.96	2.08	2.90	2.44	1.79	1.77	2.42	2.88
Age (Ma)									15.4±0.9													
$^{87}Sr/^{86}Sr$	0.71025		0.70511					0.70366	0.7039	0.70372									0.70411			0.70528
$^{87}Rb/^{86}Sr$	4.56184		0.85538					0.06435		0.05501									0.75112			0.35053
$^{143}Nd/^{144}Nd$	0.512841		0.512868					0.512868	0.512871	0.512902									0.512847			0.512801
$^{147}Sm/^{144}Nd$	0.12157		0.14139					0.14346	0.14084	0.15286									0.11901			0.12816
ε_{Nd}[3]	4.9		5.2					5	4.7	5.3									4.3			3.4
Easting	332694	340453	333270	333398	323955	331456	331799	341115	362505	360278	329528	373215	358759	357060	355756	369271	401933	366092	366138	366138	357638	402516
Northing	6382660	6398651	6403138	6432279	6391475	6469672	6469552	6432033	6386025	6385561	6440846	6311865	6209792	6209147	6208357	6282557	6255896	6406269	6405920	6405920	6364778	6356991

TABLE 1. *(Cont.)*

	Abanico Formation							Farellones Formation													La Copa rhyolite	
	CA65	CN1	CN9	CN27	CN37	CN40	CN41	CA3	CA13	CV12	CA19	CA24	CA28	CA29	CE21	CE23	CE43	CE44	CE45	CE51	CA30	CA33
SiO_2 (wt %)	57.35	57.03	52.11	51.85	63.18	64.86	52.77	52.99	56.04	60.55	50.95	66.21	63.55	56.77	51.41	51.09	50.46	53.73	55.18	57.57	70.78	71.13
TiO_2	0.72	0.70	1.10	0.71	0.60	0.43	1.50	1.07	1.01	0.92	1.15	0.72	0.73	1.15	1.45	1.41	1.21	0.97	0.90	0.91	0.21	0.21
Al_2O_3	19.19	20.04	18.81	20.18	18.69	17.67	16.19	18.94	17.69	17.97	19.66	14.98	17.07	18.28	18.14	18.35	18.91	20.21	18.87	18.88	16.72	16.48
Fe_2O_3	7.04	6.97	9.71	8.57	4.37	4.24	13.55	8.84	7.85	6.22	9.92	5.82	5.37	9.87	10.93	10.75	10.79	7.91	8.25	7.53	1.41	1.35
MnO	0.13	0.13	0.18	0.14	0.05	0.11	0.25	0.26	0.33	0.13	0.19	0.14	0.11	0.22	0.18	0.19	0.19	0.14	0.14	0.16	0.04	0.02
MgO	4.02	1.74	4.28	5.33	1.60	1.42	4.15	4.85	4.43	2.00	4.09	1.34	2.27	1.91	3.68	3.81	3.52	2.97	3.66	3.27	0.44	0.51
CaO	5.35	6.98	8.84	8.77	4.88	3.63	6.66	7.37	5.65	5.20	9.77	3.58	3.86	5.10	8.67	8.95	10.66	8.88	7.75	7.46	2.35	2.03
K_2O	1.42	1.20	1.22	0.94	1.45	1.77	0.51	1.44	2.25	1.84	0.56	2.76	2.08	1.45	1.23	1.20	0.55	1.06	1.14	0.35	2.71	3.26
Na_2O	4.44	4.78	3.52	3.34	4.98	5.57	4.17	3.94	4.50	4.81	3.48	4.18	4.58	4.89	3.96	3.92	3.39	3.86	3.89	3.61	5.27	4.93
P_2O_5	0.33	0.44	0.24	0.16	0.20	0.30	0.25	0.30	0.27	0.35	0.25	0.27	0.37	0.38	0.34	0.33	0.33	0.26	0.24	0.26	0.07	0.08
LOI	2.94	2.25	1.31	2.50	3.63	1.51	3.01	1.79	2.41	3.25	2.59	2.90	2.97	2.41	1.33	0.75	2.98	1.75	3.91	1.65	2.17	1.56
Mg#[1]	0.56	0.35	0.49	0.58	0.45	0.42	0.40	0.55	0.55	0.41	0.48	0.34	0.48	0.30	0.43	0.44	0.42	0.45	0.49	0.49	0.41	0.46
Cr (ppm)	6.59	6.14	35.77	39.59	9.34	2.13	8.25	42.05	135.68	3.00	60.37	2.06	2.06	3.07	21.37	22.54	51.74	9.77	12.28	4.68	3.07	3.25
Co	17.82	20.58	27.85	28.44	11.06	6.58	29.37	31.42	25.69	11.04	29.34	6.51	6.06	14.77	28.41	30.27	36.72	19.20	24.33	4.04	2.46	1.87
Ni	7.21	5.57	11.84	25.49	7.06	2.41	7.96	45.52	68.96	2.27	14.89	2.16	1.34	2.77	14.19	14.22	34.95	8.78	6.87	10.37	1.84	2.84
Rb	31	14	17	16	23	34	8	47	55	44	8	57	43	17	32	32	8	14	14	5	108	82
Sr	929	517	485	735	819	573	534	644	740	440	495	240	438	402	534	540	556	640	527	554	788	693
Cs	0.50	0.20	0.17	1.16	4.13	1.16	0.49	1.90	0.65	2.55	0.09	0.25	0.54	0.37	0.72	1.13	3.35	14.44	2.25	1.08	39.97	10.48
Ba	678.4	998.2	606.5	237.7	624.6	558.0	254.6	431.8	602.1	454.8	213.4	516.2	470.6	662.5	346.6	336.0	270.8	366.0	395.0	264.1	816.6	814.4
Sc	10.1	21.9	31.0	23.4	7.1	4.6	44.9	21.9	19.2	18.2	32.4	16.9	11.0	22.0	32.6	30.4	30.2	19.6	24.2	14.6	2.7	3.0
V	110.7	170.9	286.2	223.8	93.8	32.3	365.7	225.2	184.4	94.4	302.3	28.3	73.3	102.6	301.6	306.8	266.7	213.6	226.7	188.0	23.6	25.2
Ta	0.79	0.17	0.15	0.08	0.17	0.31	0.20	0.30	0.38	0.39	0.22	0.54	0.36	0.35	0.27	0.25	0.22	0.19	0.19	0.26	0.24	0.23
Nb	10.82	2.56	3.04	1.23	1.76	4.16	3.30	4.58	4.92	4.65	3.18	7.00	5.05	4.71	3.45	4.03	3.30	2.65	2.39	3.15	2.66	3.05
Zr	188.8	72.2	84.9	46.7	75.4	159.2	107.3	114.5	170.6	190.7	87.3	201.6	156.7	156.7	114.6	110.5	110.8	89.6	101.0	103.9	99.4	
Hf	4.61	2.06	2.42	1.34	2.19	4.38	3.17	3.33	4.74	5.31	2.43	5.74	4.34	4.40	3.32	3.28	3.11	2.55	2.91	3.03	2.75	2.75
Th	5.36	2.44	1.41	1.17	0.74	3.20	2.06	2.95	5.74	5.39	1.54	7.31	4.43	3.96	2.85	2.92	2.06	2.22	5.20	3.25	1.74	1.73
U	1.67	0.67	0.41	0.34	0.19	0.93	0.56	0.86	1.59	1.56	0.44	2.10	1.21	0.90	0.80	0.83	0.52	0.61	1.36	0.98	1.44	1.12
Y	16.3	22.8	20.2	11.5	5.3	14.1	31.5	15.9	15.8	29.6	18.7	32.6	17.9	33.5	23.3	22.8	22.4	16.0	17.6	14.1	4.3	3.7
La	25.66	14.32	9.11	7.00	9.44	18.57	9.69	17.18	17.01	16.89	9.86	19.57	19.58	17.42	16.01	15.27	14.33	13.94	14.09	15.46	10.12	10.00
Ce	55.84	27.83	22.90	17.64	25.94	41.22	25.37	36.33	39.55	35.97	24.43	46.45	43.80	42.83	37.60	35.37	34.02	28.29	30.91	33.55	20.75	20.72
Pr	7.24	4.07	3.42	2.28	3.18	5.45	3.72	4.80	5.65	5.32	3.24	6.22	5.41	5.38	4.83	4.89	4.54	3.69	4.04	4.33	2.33	2.42
Nd	27.41	17.09	15.00	9.85	14.22	20.71	18.97	17.92	19.57	23.15	14.27	25.03	23.70	26.85	22.09	20.66	23.09	17.61	18.21	19.22	7.67	7.92
Sm	5.30	4.03	4.13	2.51	2.61	4.06	4.93	4.57	4.79	5.66	3.83	6.15	4.75	5.65	5.47	5.47	5.18	3.94	4.08	4.02	1.70	1.71
Eu	1.57	1.30	1.31	0.91	0.84	1.12	1.46	1.36	1.20	1.53	1.24	1.53	1.37	1.70	1.58	1.66	1.51	1.21	1.15	1.17	0.51	0.45
Gd	4.37	3.94	4.26	2.45	1.94	3.15	5.57	3.98	3.98	5.86	3.97	6.09	4.18	5.77	5.37	5.48	5.15	3.76	3.78	3.57	1.16	1.16
Tb	0.64	0.61	0.65	0.37	0.26	0.44	0.93	0.61	0.62	0.92	0.66	1.02	0.64	0.94	0.88	0.84	0.81	0.59	0.59	0.54	0.18	0.16
Dy	3.50	3.70	3.84	2.20	1.22	2.56	5.75	3.41	3.32	5.48	3.92	6.23	3.59	5.62	4.75	4.78	4.66	3.28	3.41	3.00	0.84	0.78
Ho	0.68	0.79	0.79	0.44	0.22	0.51	1.22	0.69	0.66	1.13	0.84	1.36	0.75	1.20	0.96	0.97	0.96	0.66	0.71	0.59	0.17	0.15
Er	1.80	2.30	2.19	1.29	0.56	1.47	3.59	1.84	1.77	3.27	2.33	3.88	2.05	3.33	2.59	2.58	2.56	1.78	1.95	1.53	0.42	0.41
Yb	1.74	2.29	2.06	1.20	0.50	1.51	3.31	1.76	1.62	3.09	2.27	3.94	2.01	3.25	2.33	2.35	2.33	1.70	1.93	1.40	0.45	0.40
Lu	0.25	0.35	0.30	0.18	0.08	0.24	0.51	0.24	0.24	0.47	0.33	0.59	0.30	0.47	0.36	0.34	0.34	0.26	0.28	0.21	0.07	0.07
La/Yb	14.71	6.24	4.42	5.81	18.81	12.31	2.93	9.79	10.49	5.47	4.35	4.97	9.75	5.35	6.87	6.50	6.16	8.21	7.32	11.07	22.53	24.91
Cu	158.5	71.1	89.2	69.4	52.5	93.7	204.4	137.1	287.2	71.0	76.5	74.7	69.7	76.9	169.3	130.0	203.3	122.0	69.0	79.9	85.3	114.8
Zn	5.4	43.9	116.7	75.3	65.8	10.8	126.2	77.8	34.4	22.5	89.3	10.0	11.5	17.8	96.3	100.3	90.8	64.4	54.2	65.5	52.2	157.0
Mo	0.73	0.97	0.65	0.65	0.51	0.70	0.56	0.82	1.19	0.74	0.60	1.43	1.01	0.85	1.17	1.31	0.89	0.86	1.83	1.32	0.75	0.60
Pb	6.80	4.40	4.15	5.13	4.77	9.54	18.77	7.94	28.49	10.03	2.67	9.89	8.97	7.07	6.99	7.15	5.57	7.53	5.72	4.78	17.99	14.83

TABLE 1. *(Cont.)*

	Abanico Formation							Farellones Formation										La Copa rhyolite	
	CA65	CN1	CN9	CN27	CN37	CN40	CN41	CA3	CA13	CV12	CA19	CA24	CA28	CA29	CE21	CE23	CE43	CE44	CE45	CE51	CA30	CA33
La/Yb_n[2]	10.55	4.48	3.17	4.17	13.49	8.83	2.10	7.02	7.52	3.93	3.12	3.56	6.99	3.84	4.93	4.66	4.42	5.88	5.24	7.94	16.15	17.86
La/Sm_n	3.12	2.30	1.43	1.80	2.34	2.95	1.27	2.43	2.29	1.93	1.66	2.05	2.66	1.99	1.89	1.80	1.79	2.29	2.23	2.49	3.85	3.77
Gd/Yb_n	2.07	1.42	1.71	1.68	3.20	1.73	1.39	1.88	2.03	1.57	1.45	1.28	1.72	1.47	1.90	1.93	1.83	1.83	1.62	2.12	2.14	2.39
Sm/Yb_n	3.38	1.95	2.23	2.31	5.78	2.99	1.65	2.89	3.28	2.04	1.88	1.74	2.63	1.93	2.61	2.58	2.47	2.58	2.35	3.20	4.20	4.74
Age (Ma)					21.9±2.2										12.4±1.7			10.9±1.6	11.6±1.5			
$^{87}Sr/^{86}Sr$					0.70379		0.70379		0.70399						0.70397			0.70397	0.70414		0.70429	
$^{87}Rb/^{86}Sr$							0.04405		0.21737										0.07675			
$^{143}Nd/^{144}Nd$					0.512875		0.512909		0.512824						0.512829			0.512824	0.512789		0.512721	
$^{147}Sm/^{144}Nd$					0.11109		0.15702		0.14797						0.14546			0.14003	0.13535		0.10735	
ε_{Nd}[3]					4.9		5.4		3.7						3.8			3.7	3		1.7	
Easting	401015	357033	360736	364167	355172	357339	357339	382664	382806	375953	363374	369107	382881	378555	367171	368524	377666	377679	377679	369565	381726	381536
Northing	6357108	6373858	6374247	6404203	6380382	6384670	6384670	6325739	6329260	6284829	6307314	6306589	6308109	6307593	6210416	6210389	6213631	6213732	6213732	6226248	6332690	6332325

[1] Mg# is calculated as $Mg/(Mg+Fe^{2+})$, where Fe^{2+} is assumed to be 90% of the total Fe content

[2] La/Yb_n, La/Sm_n, Gd/Yb_n and Sm/Yb_n are chondrite normalized using the values of Sun and McDonough (1989)

[3] ε_{Nd} is calculated as follows: $\varepsilon_{Nd(t)} = [[(^{143}Nd/^{144}Nd)_{sample}(t)]/[(^{143}Nd/^{144}Nd)_{CHUR}(t)]-1] \times 104$ where $(^{143}Nd/^{144}Nd)_{CHUR} = 0.512638$

Samples grouped herein as the Abanico Formation are predominantly basaltic andesite and andesite (26 out of 35 samples) but range from basalt to rhyolite (SiO_2 = 51–75 wt %; Table 1). The samples can be subdivided into two distinct suites. Those from south of 33.5° S, traditionally assigned to the Coya Machalí Formation (Fig. 1), are tholeiitic basalt and basaltic andesite (Fig. 2), whereas those from areas to the north, and traditionally assigned to the Abanico and Los Pelambres Formations (Fig. 1), are largely calc-alkaline basalt and andesite. The southern suite is LREE enriched (La/Sm_n = 1.8–2.5) with moderately fractionated HREE (Sm/Yb_n = 1.7–4.0; Fig. 3), whereas the northern suite is characterized by greater LREE enrichment (La/Sm_n = 1.3–4.1) and, in part, stronger HREE fractionation (Sm/Yb_n = 1.5–5.8; Fig. 3).

Most of the samples from the Salamanca Formation, taken from outcrops east of the Pocuro fault, range from basalt to basaltic andesite, and only one rhyolitic unit was sampled (SiO_2 = 51–71 wt %; Table 1). Most are calc-alkaline, but two fall in the tholeiitic field in Figure 2. The samples are LREE enriched (La/Sm_n = 1.5–2.7) with moderately fractionated HREE (Sm/Yb_n = 1.6–2.7; Fig. 3). Minor variations in the large ion lithophile elements (LILE, Rb, and Sr) are attributed to the greater mobility of these elements during alteration.

Twenty samples of the Farellones Formation were analyzed. They comprise basalts and andesites (SiO_2 = 50–63 wt %; Table 1) and straddle the boundary between the tholeiitic and calc-alkaline fields (Fig. 2). As with the other samples, the rocks of the Farellones Formation are LREE enriched (La/Sm_n = 1.7–2.5) and exhibit moderately fractionated HREE (Sm/Yb_n = 1.7–3.2; Fig. 3).

The rocks of the La Copa rhyolite complex (SiO_2 = 70–71 wt %), exposed on the western side of the Río Blanco-Los Bronces porphyry center, are characterized by pronounced LREE enrichment (La/Sm_n = 3.8–3.9) as well as slightly more fractionated HREE (Sm/Yb_n = 4.2–4.7; Fig. 3) than most of the older samples.

Geochronology

Mineral separates were dated from single volcanic units of the Abanico (locally, Los Pelambres) and Salamanca Formations and from a volcanic flow and two dikes assigned to the Farellones Formation. Hornblende from sample CN37 was dated in order to constrain the age of the lower section of the Los Pelambres Formation. The age spectrum (Fig. 4A) is disturbed, with the apparent age climbing to a final step at 21.9 ± 2.2 (2σ) Ma. This is interpreted as a minimum age for crystallization, with the lower temperature steps recording outgassing. This age is broadly consistent with other ages derived from the Los Pelambres Formation north of Río Blanco (Rivano et al., 1993).

Data from Ar-Ar step-heating analysis of plagioclase phenocrysts from the Salamanca Formation, sample CN46, are presented in Figure 4B. The eight-step analysis yielded a plateau with an age of 15.4 ± 0.9 (2σ) Ma, representing 79 percent of the Ar released. This is younger than a published whole-rock K-Ar age of 22 Ma for a unit ~1 km to the west (Rivano et al., 1993) but is broadly consistent with the reported age range for the Salamanca Formation in this area (Fig.1; Rivano et al., 1993). Overall there appears to be a temporal overlap between the Salamanca and Farellones Formations in the area east of the Pocura fault.

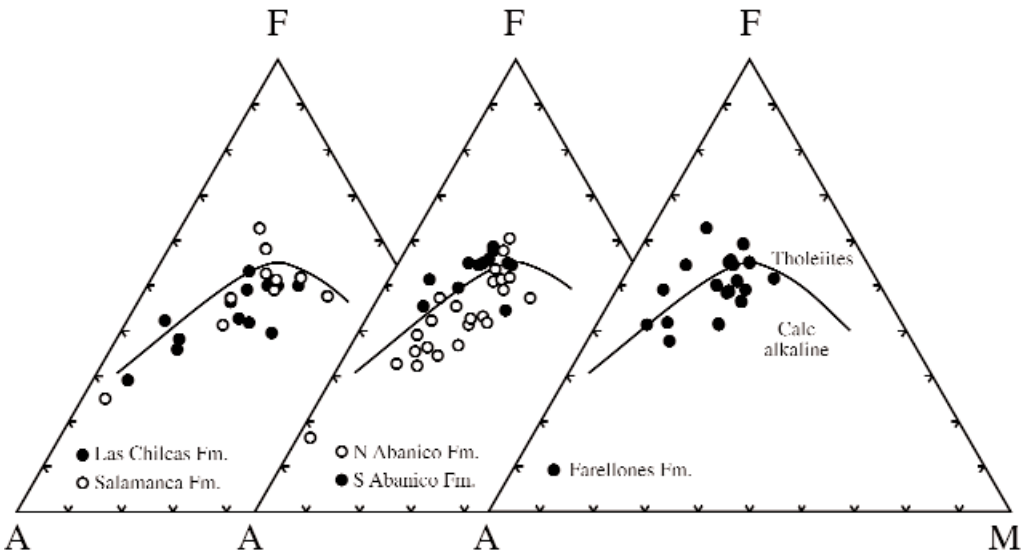

FIG. 2. AFM ternary diagrams for the differentiation of tholeiitic and calc-alkaline rock series for the Tertiary volcanic rocks of this study. Older suites are predominantly calc-alkaline, whereas the younger Abanico and Farellones Formations include both calc-alkaline and tholeiitic rocks. A = $Na_2O + K_2O$, F = total iron as FeO, M = MgO.

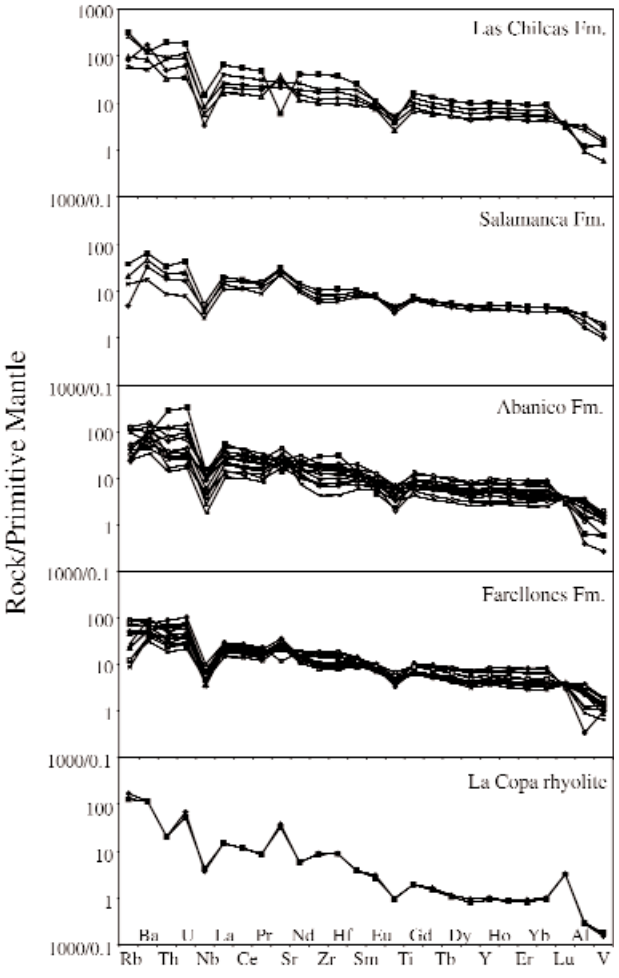

FIG. 3. Primitive-mantle normalized plots for representative volcanic rocks from this study, showing the broad similarity between the rocks of the Las Chilcas, Salamanca, Abanico, and Farellones Formations. Normalizing values are those of Sun and McDonough (1989).

Samples CE21, CE44, and CE45 were selected to constrain the age of the upper successions of the Farellones Formation in the vicinity of the abandoned La Juanita copper mine, south of El Teniente (Fig. 1). Samples CE44 and CE45 are andesitic dikes from north of the mine, whereas sample CE21 is an olivine-phyric basalt from the Río Pangal valley ~15 km west of the mine. O. Rivera and M. Falcon (1998, unpub. report for CODELCO-Chile, 200 p.) have reported a K/Ar whole-rock age of 11.9 ± 0.5 Ma for the Río Pangal-Río Paredones volcanic sequence, 1 km to the east of sample CE21. The hornblende from sample CE45 yielded only two steps (Fig. 4C) and the imprecise date of 11.6 ± 3.0 Ma should be regarded as a total-fusion age. However, the plagioclase from samples CE44 and CE21 yielded more steps (Fig. 4D, E) and acceptable plateau ages of 10.9 ± 1.6 and 12.4 ± 1.7 Ma, respectively, similar to the hornblende date. Both samples display u-shaped Ca/K ratio trends (Fig. 4), possibly as a result of sericitic alteration of the plagioclase. The similar ages for the three samples suggests that they represent magmatic cooling ages. The andesitic dikes were intruded at ~11 Ma and therefore are broadly synchronous with published ages for the surrounding volcanic units (e.g., the Río Pangal-Río Paredones sequence) and are also geochemically similar to these rocks (Table 1, Fig. 3; O. Rivera and M. Falcon, 1998, unpub. report for CODELCO-Chile, 200 p.). The inferred age range of these rocks (ca. 11–12.5 Ma) overlaps with that determined by S. Kay and A. Kurtz (1995, unpub. report for CODELCO-Chile, 180 p.) for the upper part of the Maqui Chico Group in the El Teniente area.

Radiogenic isotopes

Fourteen samples were analyzed for Rb-Sr and Sm-Nd isotopes (Table 1). $^{87}Sr/^{86}Sr$ ratios vary from 0.70366 to 0.71025, but the majority fall in the range of 0.70366 to 0.70429. There is no clear trend in initial ratio through the eruption of the Abanico, Salamanca, and Farellones Formations (i.e., from early to middle Miocene). We calculated ε_{Nd} values using the

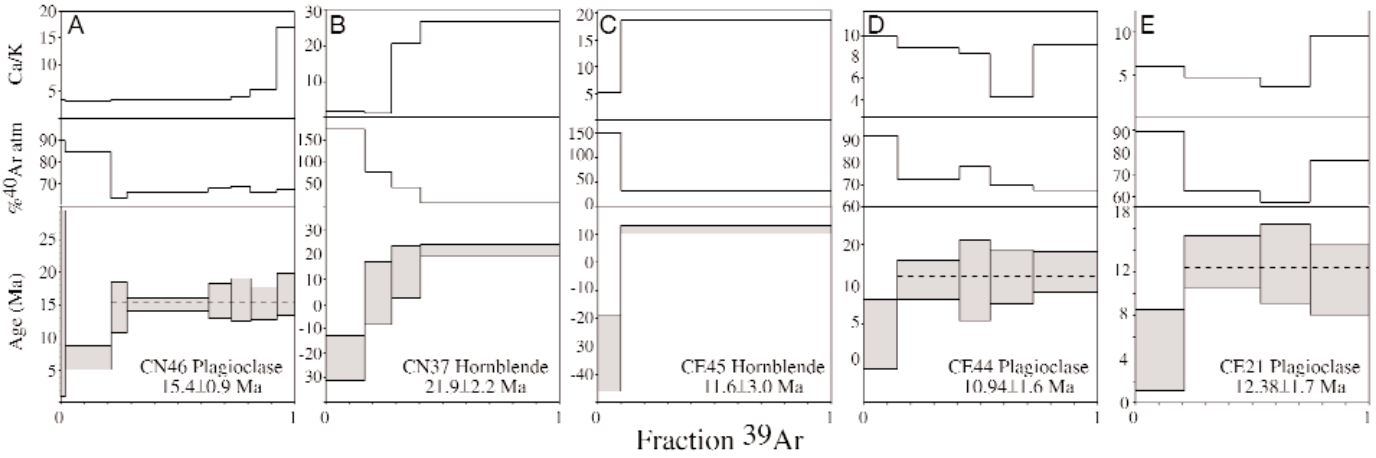

FIG. 4. Ar-Ar age spectra and related data for samples analyzed in this study. Ages are plateau ages with errors reported to 2σ (see App.).

new age data reported herein or previously published ages for adjacent mapped units. Positive ε_{Nd} values (1.7–5.2) are indicated by all samples. The values are lower for the Farellones Formation (3.0–3.8, n = 4) than for the older Abanico (3.4–5.4, n = 4) and Salamanca (4.7–5.3, n = 3) Formations. The Sr and Nd isotope data are therefore decoupled for these units. The Cretaceous Las Chilcas Formation (n = 2) contains more radiogenic Sr (0.70511 and 0.71025, n = 2) but has higher ε_{Nd} (4.9–5.2) than the Miocene rocks. The Pliocene La Copa rhyolite is only slightly more enriched in ^{87}Sr than most of the Miocene units (0.70429, n = 1) but has the lowest ε_{Nd} value (1.7), which is still significantly higher than the range of values reported by Nyström et al. (1993).

Three of the four samples from the Abanico Formation plot within the range of the data of S. Kay and A. Kurtz (1995, unpub. report for CODELCO-Chile, 180 p.) for the Coya Machalí Formation in the El Teniente region. Sample CA60, however, has a markedly higher $^{87}Sr/^{86}Sr$ ratio (0.71025), as well as a lower ε_{Nd} value (3.4) than the other samples, and is inferred to record contamination by older crustal material. Similarly, the radiogenic isotope data for the three samples from the Salamanca Formation are within the ranges reported for the Coya Machalí Formation by S. Kay and A. Kurtz (1995, unpublish. report for CODELCO-Chile, 180 p.; Fig. 5).

Discussion

The Cretaceous to middle Miocene volcanic rocks analyzed in this study have broadly similar major and trace element compositions, characterized by LREE enrichment, negative Nb anomalies in primitive mantle-normalized diagrams (Fig. 3), and La/Ta ratios generally exceeding 25 (Table 1). All features are characteristic of magmas derived ultimately from a sub-arc mantle source (e.g., Kay and Mpodozis, 2002). The observed depletion of HFSE (Nb, Ta, Hf, Zr, Ti), and especially the Nb-Ta trough (Fig. 3), is also characteristic of this tectonic environment. The youngest analyzed rocks, the Pliocene La Copa rhyolites, also have geochemical characteristics of arc magmas, but they exhibit distinctive REE compositions.

Earlier workers in the area, and particularly S. Kay and A. Kurtz (1995, unpub. report for CODELCO-Chile, 180 p.) and Kay et al. (1999, 2005), reported similar geochemical characteristics. However, because the three major Miocene-Pliocene porphyry copper-molybdenum deposits in the region lie in different settings relative to the major warp in the subducting plate and may have been generated in different environments as the plate flattened, we subdivide our geochemical data into three populations, corresponding to the areas surrounding, respectively, the Los Pelambres, Río Blanco-Los Bronces, and El Teniente deposits, (i.e., 31°45' S–32°45' S; 32°45' S–33°30'S; 33°30' S–34°15' S). We combine these new results with data from the same areas previously reported by Skewes and Stern (1995), S. Kay and A. Kurtz (1995, unpub. report for CODELCO-Chile, 180 p.), Reich et al. (2003), Nyström et al. (2003), and Kay et al. (2005). The geochronologically well-constrained analytical database of Bissig et al. (2003) for the El Indio-Pascua Au belt to the north of the study area provides a template for the geochemical response to slab-flattening and is used as a comparison for the evolution of the more southerly transects.

Crustal thickening in central Chile

The history of crustal thickening through the Miocene is clearly documented for the axial flat-slab transect by the geomorphologic studies of Bissig et al. (2002), which support the tectonic studies of Kay et al. (1991) and Martin et al. (1995). Farther south, S. Kay and A. Kurtz (1995, unpub. report for CODELCO-Chile, 180 p.) and Kurtz et al. (1997) extended the tectonic reconstruction of Godoy and Lara (1994) with ^{40}Ar-^{39}Ar and aluminum-in-hornblende studies of the cooling and exhumation history of two Miocene plutons (19.6 and 8.4 Ma, respectively) in the El Teniente region and with similar data for units of the San Francisco batholith (ca. 8.6–20.1 Ma), which hosts the Río Blanco-Los Bronces porphyry center (Skewes and Holmgren, 1993). These studies employed radically different approaches to recognize episodes of uplift, exhumation, and, hence, crustal thickening in the early Miocene (ca. 15–19 Ma) and late middle Miocene (6–10 Ma). Uplift and crustal thickening during the intervening period (12.5–14 Ma) are recorded geomorphologically in the El Indio transect. Although this has not been confirmed in the Río Blanco-Los Bronces and El Teniente mine areas for the

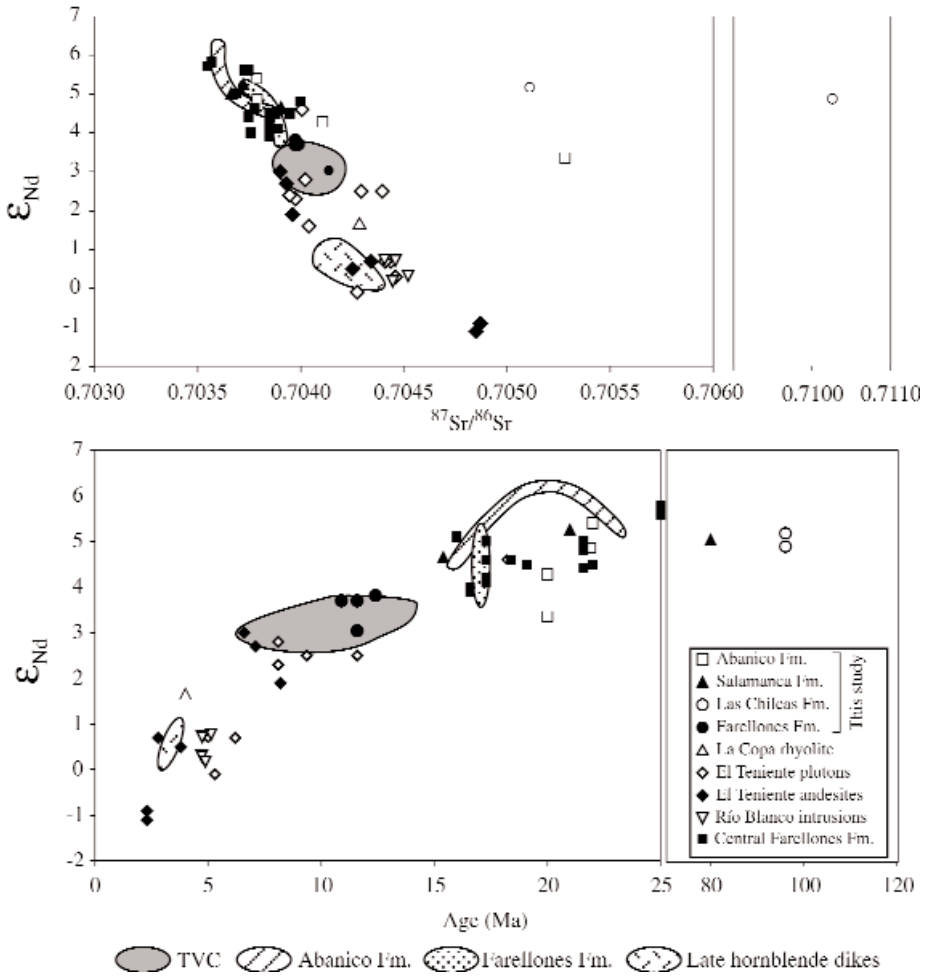

FIG. 5. A. ε_{Nd} vs. $^{87}Sr/^{86}Sr$. B. ε_{Nd} vs. age for Tertiary volcanic rocks from this study compared to regional data sets of Kay et al. (2005) and S. Kay and A. Kurtz (1995, unpub. report for CODELCO-Chile, 180 p.; shaded fields). The general decrease in ε_{Nd} over time is consistent with increased assimilation of crustal material in the sub-arc mantle. TVC = Teniente volcanic complex. Data for the El Teniente plutons, Teniente volcanic complex, and late hornblende dikes are from S. Kay and A. Kurtz (1995, unpub. report for CODELCO-Chile, 180 p.). Data for El Teniente andesites and Río Blanco intrusions are from Stern and Skewes (1995). Data for the central Farellones Formation are from Nyström et al. (2003).

same time period, it is apparent that the Miocene tectonic histories of the axis and southern boundary of the flat-slab domain were similar, providing a coherent regional framework for comparison of the geochemistry.

Kay et al. (1999) and Kay and Mpodozis (2001) argued for a direct link between Neogene crustal thickening, igneous geochemistry, and mineralization. This link is also discussed by Kay et al. (1999) and Bissig et al. (2003) for the El Indio-Pascua epithermal Au(-Ag, Cu) belt (ca. 30°S), now at the center of the Chilean flat-slab domain, north of the present study area. In contrast, Stern and Skewes (1995) proposed that magma compositional trends in the volcanic rocks reflect the tectonic erosion and subduction of the diverse lithologies making up the leading edge of the South American plate.

Rare earth element geochemistry

It is relevant to subdivide the igneous suites into those which predated hydrothermal activity (i.e., the Las Chilcas through Farellones Formations > ~11 Ma), and those which were associated with or closely followed ore formation. All samples from the Upper Cretaceous to middle Miocene Las Chilcas, Abanico, Salamanca, and Farellones Formations exhibit similar REE patterns (Fig. 3). They are LREE enriched (La/Sm_n ranging from 1.5–4.1 but with most values <2.5) and exhibit only moderately fractionated HREE (Sm/Yb_n = 1.5–5.8, with most values <2.5; Fig. 3). Thus the volcanic and hypabyssal rocks erupted over almost 100 m.y. were remarkably uniform. Although most rocks are calc-alkaline, the basalts and basaltic andesites of the more southerly Abanico (Coya Machalí) Formation basalts and basaltic andesites and some of the mafic units of the Salamanca Formation are tholeiitic, and basalt and andesite of the Farellones Formation lie along the tholeiitic-calc-alkaline boundary (Fig. 2). The greatest LREE enrichment (La/Sm_n = 4.1) and HREE fractionation (Gd/Yb_n = 5.8) occur in the calc-alkaline rocks of the more northerly Abanico Formation.

These data indicate that, with few exceptions, the central Chilean arc had a consistent REE chemistry from the Late

Cretaceous to the late middle Miocene. Previous investigations have suggested that whereas the Coya Machalí (Abanico) Formation is dominantly tholeiitic, a trend to more calc-alkalic compositions occurred during the eruption of the Farellones Formation (S. Kay and A. Kurtz, 1995, unpub. report for CODELCO-Chile, 180 p.). Our data show that calc-alkalic compositions occur in the majority of the rocks from the more northerly Abanico (Los Pelambres) Formation. Furthermore, the geochemistry of the Abanico and Farellones Formations is transitional rather than abrupt, as proposed by Charrier et al. (2002), and contrasts with the gradual change in the nature of the source region for these suites since ~26 Ma argued by others (e.g., Kay et al., 1999; Kay and Mpodozis, 2001, 2002).

Yáñez et al. (2002) described the Abanico Formation between 33° and 35° S as being tholeiitic with low La/Yb ratios and less LILE enrichment than other volcanic units of central Chile. Together with the absence of hydrous mineral phases, this was interpreted as indicating low primary water contents in the magmas. The transition from tholeiitic rocks in the south to more calc-alkaline rocks in the north implies a change in the nature of the mantle source of the parental magma from southern to northern central Chile during the Miocene. Yáñez et al. (2002) interpreted the tholeiitic nature of the southern portion of the Abanico Formation as reflecting a diminished fluid supply from the downgoing slab, possibly as the result of its detachment south of the Juan Fernández Ridge. The north-south transition from calc-alkaline to tholeiitic volcanism in the Abanico Formation supports this model and the idea that the processes by which parental magmas were generated and the depth at which this occurred was controlled by geographically localized processes associated with the margin of the flat slab rather than crustal thickening.

S. Kay and A. Kurtz (1995, unpub. report for CODELCO-Chile, 180 p.) and Kay and Mpodozis (2001, 2002) have documented a gradual trend to increasing LREE abundances and HREE fractionation with decreasing age for the ~25 to ~5 Ma rocks in the vicinity of El Teniente. This was interpreted to be the result of increasing crustal thicknesses and a change from a pyroxene- to an amphibole- and finally a garnet-dominated lower crustal mineral assemblage. However, our regional data set shows very little difference in the LREE (La/Sm_n) or HREE (Sm/Yb_n) ratios between the Cretaceous Las Chilcas and the Miocene Abanico and Farellones Formations (Fig. 3, Table 1). Rather, the La/Yb ratios do not vary until the Pliocene with the peak La/Yb values migrating southward over time (Fig. 6)

When compared with data from the flat slab region of central Chile (Bissig et al., 2003) significant differences can be observed. Unlike the Miocene porphyry belt discussed in this study, samples from the El Indio belt show a gradual increase in La/Yb ratios in younger rocks, starting at values comparable to those of the Miocene porphyry belt, reaching a peak La/Yb ratio of ~40 at ~7 Ma before dropping to much lower values (Fig. 6). Bissig et al. (2003) interpreted the geochemical trends in the El Indio belt to be consistent with crustal thickening but observed that this thickening and associated large-scale breakdown of amphibole was not the key control on ore deposit formation. The absence of a gradual increase in the La/Yb ratios south of the current flat slab suggests that gradual crustal thickening was not important and that an

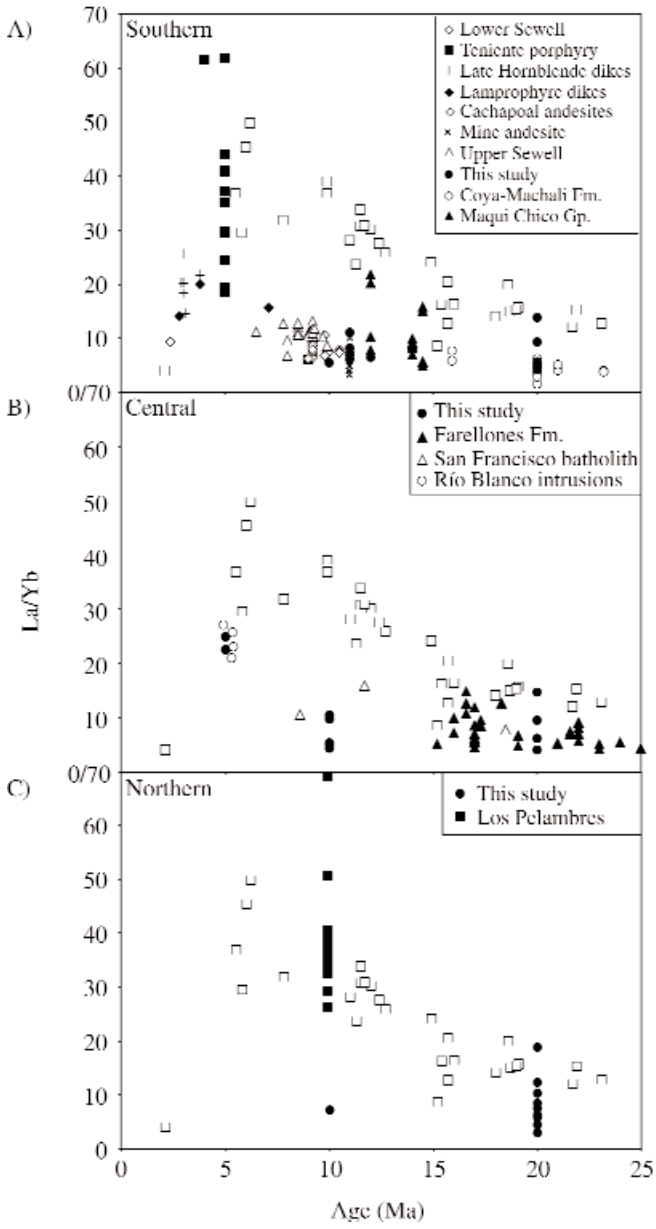

FIG. 6. Age vs. La/Yb for Tertiary igneous rocks of central Chile, illustrating the rapid rather than gradual increase in La/Yb around the time of significant mineralization, compared to the gradual increase in La/Yb shown by rocks from the El Indio-Pascua area. In all three plots open squares are data for the El Indio-Pascua belt from Bissig et al. (2003). A. Southern transect (33°30'–34°15' S). Data from this study include samples of the Abanico and Farellones Formations. Data for the mine andesite are from El Teniente mine (A. Skewes, 1997, unpub. report for CODECLO-Chile, 11 p.; A. Skewes, 1998, unpub. report for CODECLO-Chile, 15 p.). Data for the Cachapoal andesite are from Stern and Skewes (1995). All other data are from Kay et al. (2005) and S. Kay and A. Kurtz (1995, unpub. report for CODELCO-Chile, 180 p.). B. Central transect (32°45'–33°30' S). Data from this study include samples from the Abanico and Farellones Formations and the Pliocene La Copa rhyolite. Data for the San Francisco batholith from Skewes (1992) and Stern and Skewes (1995). Data for the Río Blanco intrusions from Stern and Skewes (1995). Data for the Farellones Formation, other than those from this study, are from Nyström et al. (2003), Kay et al. (2005), and S. Kay and A. Kurtz (1995, unpub. report for CODELCO-Chile, 180 p.). C. Northern transect (31°45'–32°45' S). Data from this study include samples from the Abanico and Farellones Formations. Data for the Los Pelambres area are from Reich et al. (2003).

abrupt shift in the nature of the source regime at ~10 Ma near Los Pelambres and ~4 to 5 Ma south of Río Blanco was more likely (Fig. 6). The change in the geochemistry of the volcanic rocks in the vicinity of the northern transect occurred at approximately the same time as the shift to a strongly compressional tectonic regime in the magmatic arc of central Chile (31–34° S; Kurtz et al., 1997; Yáñez, et al., 2002); however, the younger geochemical shift to the south does not appear to be related to any major tectonic event. The fact that the peak in La/Yb occurred at the same time in the vicinity of both El Teniente and Río Blanco is consistent with the new age data for the deposits, which suggests they are broadly coeval (Cannell et al., 2003; Deckart et al., 2005).

Radiogenic isotopes and crustal contamination

Various authors have observed a trend of increasing $^{87}Sr/^{86}Sr$ and decreasing ε_{Nd} values with time in the volcanic and intrusive rocks of central Chile (e.g., Stern and Skewes, 1995; Kay et al., 1999). This trend requires incorporation into the parental magma of an older, isotopically distinct component, but the source of this older material remains the subject of considerable debate. Some workers have argued for crustal contamination within the lower continental crust (Hildreth and Moorbath, 1988; Kay et al., 1999), whereas others have argued for incorporation of crustal material into the sub-arc mantle source region (Stern, 1989; Stern and Skewes, 1995). The regional Miocene and Pliocene samples from this study, which are comparable to those documented at El Teniente by Kay et al. (1999), are not characterized by systematic variations in either major or trace element geochemistry. Furthermore, although ε_{Nd} values decrease and $^{87}Sr/^{86}Sr$ increases with age (Fig. 5), the younger Farellones Formation samples do not have systematically higher SiO_2 or Sr contents than the older samples analyzed in this study (Table 1). This argues against contamination by intracrustal assimilation combined with fractional crystallization, as this process would result in elevated SiO_2 and Sr. Instead, Stern (1991) has shown that incorporation of only 1 percent of tectonically eroded Paleozoic basement into the sub-arc mantle could generate andesites with Sr isotope signatures comparable to those of the northern Southern Volcanic zone. Indeed, Kay et al. (1999) observed that the enriched isotopic signatures in Pliocene to Recent mafic volcanic rocks in the central Andes cannot be attributed to pre-Miocene processes. Taken in conjunction with the geographic distribution of enriched and depleted isotopic signatures, they suggested that not all of the isotopic enrichment can be the result of crustal contamination and that there must be some enrichment of the mantle source. Localized assimilation of crustal material within the mantle wedge as a result of subduction erosion adjacent to a zone of ridge subduction best accounts for the geochemical trends observed in this study and is consistent with the proposed subduction erosion model of Skewes and Stern (1995).

Implications for the Formation of Giant Porphyry Copper Deposits

For the latter part of the twentieth century, the three giant Cu-Mo porphyry centers of central Chile were considered to young progressively southward (e.g., Quirt et al., 1971; Sillitoe, 1988) based on the available geochronological data (e.g., 10 Ma ages of Los Pelambres-El Pachón: Kay et al., 1999; 7 Ma ages of Río Blanco-Los Bronces: Warnaars et al., 1985; 5 Ma ages of El Teniente: Cuadra, 1986). Mineralization is inferred to have been coincident with the southward migration of the flat-slab segment in central Chile. This apparent temporal and spatial association led to considerable speculation as to the role of slab flattening in the genesis of giant orebodies. However, the most recent geochronological studies have shown that this relationship is not clear-cut, with mineralization at Río Blanco temporally overlapping the emplacement of dacitic porphyries with ages from 6.32 ± 0.09 to 5.23 ± 0.07 Ma (Deckart et al., 2005), while at El Teniente mineralization occurred at ~4.7 to 5.9 Ma (Muniziga et al., 2002; Maksaev et al., 2002; Cannell et al., 2003). The overlap in the ages implies near-simultaneous formation of the two giant orebodies. Furthermore, Ar-Ar step-heating data for adularia from the Rosario breccia of the Rosario de Rengo prospect, ~80 km south of El Teniente, yield ages of 7.49 ± 0.16 and 7.58 ± 0.20 Ma (A.H. Clark, unpub. data). These results require modification of the currently accepted model for tectonic controls on ore formation in central Chile. The following discussion evaluates current models that relate slab flattening and ridge subduction to ore genesis in the light of these new geochronological and geochemical data.

Kay et al. (1999) and Kay and Mpodozis (2001) argued that all of the major Neogene central Andean copper and gold deposits formed in areas of thickened crust, where uplift was associated with crustal shortening over a shallowing subduction zone at a time of waning magmatism. They further speculated that increasing crustal thicknesses and the associated change in the residual mineralogy from amphibole- to garnet-dominated assemblages released large volumes of H_2O that may have played a role in the formation of the deposits in the Maricunga and El Indio belts. Clearly this model is of considerable importance to explorationists, as it offers a potential method for identifying packages of rocks that may be hosts for significant copper and gold deposits. However, Skewes and Stern (1995) have shown that the large volumes of fluid released by the amphibole to garnet transition during crustal thickening are not required to form large porphyry copper deposits, and the data presented in this study suggest that crustal thickening was not a critical factor in the magmatic evolution of the central Chilean porphyry belt. Stern and Skewes (1995) further argued that there is no temporal correlation between the isotopic composition of Andean magmas and crustal thickness. Because ridge subduction enhances the effects of subduction erosion (Cande and Leslie, 1986; von Huene et al., 1997), Stern and Skewes (1995) concluded that increased subduction erosion rather than crustal thickening was responsible for the geochemical and isotopic variations observed in the region.

Although there is evidence that crustal thickening has occurred in central Chile since the middle Miocene (Allmendiger et al., 1990; Kay et al., 1991), data from this study suggest that an abrupt rather than a gradual geochemical shift occurred. During the early Miocene, the Juan Fernández Ridge is interpreted to have collided with the continental margin as a result of oblique convergence of the Farallon and South American plates, with the locus of the collision migrating southward at ~200 km/m.y. (Yáñez et al., 2001). Following the

breakup of the Farallon plate at ~25 Ma the interaction between the Nazca and South American plates evolved from an oblique to an almost normal convergence, resulting in only ~275 km of south-directed migration of the ridge collision in the last 12 m.y. (Yáñez et al., 2002).

Data from this study and others (e.g., Stern and Skewes, 1995) is consistent with increased crustal contamination of the sub-arc mantle, as a result of slab flattening and a reduction in the size of the mantle wedge. In addition to the enhanced subduction erosion and crustal thickening in central Chile associated with the collision of the Juan Fernández Ridge (Stern and Skewes, 1995; von Huene et al., 1997), the ridge itself may have contributed directly to the formation of the giant orebodies. Yáñez et al. (2002) have proposed that passive ridge subduction may be a contributor to the generation of magmas beneath an arc because of the high volatile content and the large volumes of oceanic crust within the root of the ridge. In addition to magma generation, analogue modeling of seamount subduction (Dominguez et al., 2000) has demonstrated that considerable sediment may be subducted behind irregularities on the ridge. Once subducted this water-laden sediment may be underplated to the overlying continental crust where it can contribute to the hydration and oxidation of the mantle and possibly become a significant source of both fluids and metals.

Concluding Remarks

The general absence of coeval volcanism associated with porphyry copper deposits means that genetic models must extrapolate from adjacent rocks to infer the tectonic setting. Data from this study demonstrate that geochemical trends observed on a district scale differ from those observed at a more regional scale, where there is evidence for a relatively consistent source region for the volcanic rocks from the Cretaceous to the Pliocene. Similarly, radiogenic isotopes suggest a uniform source region prior to ~15 Ma, with the Farellones Formation showing the first evidence for contamination by older crustal material that is not reflected in the trace element geochemistry. This is best interpreted as the result of incorporation of older crustal material in the mantle wedge as a result of ridge subduction and slab flattening. We suggest that the subduction of the Juan Fernández Ridge may have played a greater role in the changes in the mantle source than crustal thickening, and, therefore, ridge subduction may be more important for giant ore deposit genesis than slab flattening. Figure 7 illustrates the migration of the Juan Fernández Ridge over the past 12 m.y. in a north-south schematic section and shows that the location of the flexure between normal and flat subduction may have had a considerable impact on transient low-angle reverse faulting and ore deposit formation. In

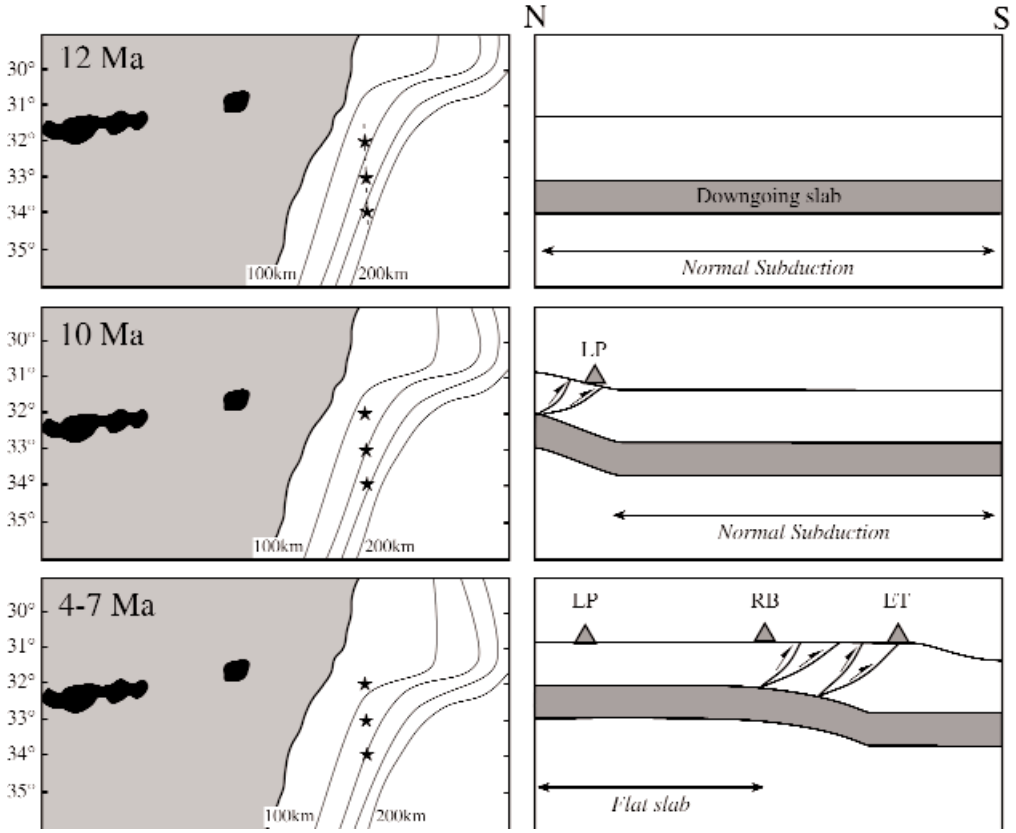

FIG. 7. Schematic diagram illustrating the southward progression of the Juan Fernández Ridge and the central Chile flat slab zone over the past 12 m.y. based on Yanez et al. (2002). Depth contours of seismicity (25-km interval) from Cahill and Isacks (1992) are shown and can be used to infer the upper surface of the downgoing slab. Stars illustrate the locations of the three major porphyry copper deposits. From north to south, these are Los Pelambres-El Pachon (LP), Río Blanco-Los Bronces (RB), and El Teniente (ET). The dashed line in the top panel shows the location of the north-south cross sections in the right-hand panels. These cross sections show inferred southward progression of the flexure that separates zones of normal and flat subduction and potential structural controls on ore deposit localization and formation.

addition, the current location of the steepest flexures in the Nazca plate lie beneath the two areas of highest topographic elevation in central Chile and Argentina, suggesting a strong link between the shape of the downgoing slab and thrust tectonics in the upper crust (Fig. 8). Ridge subduction may be responsible for both increased subduction erosion and increased sediment input in the mantle wedge, all of which may contribute to the generation of giant ore deposits.

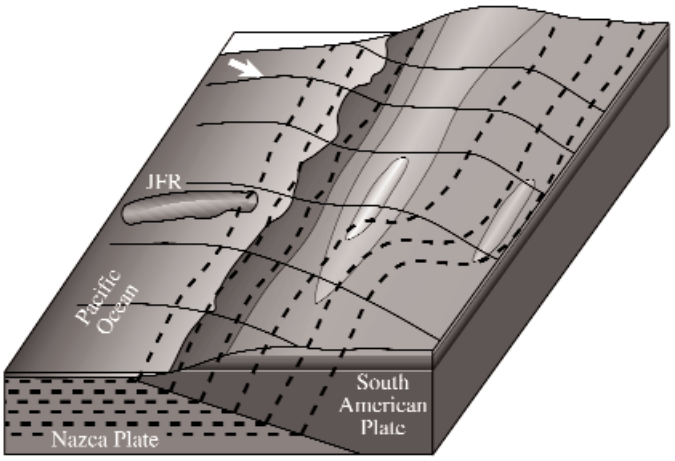

FIG. 8. Schematic block diagram illustrating the current geometry of the subducting Nazca plate and its relationship to surface topography (shaded) in central Chile. Dashed lines = contour lines for the upper surface of the downgoing plate, solid lines = form lines illustrating the geometry of the slab. Note the spatial association between topographic highs and flexure zones in the downgoing slab. JFR = Juan Fernández Ridge. Arrow is the current convergence direction from Yanez et al. (2002).

Acknowledgments

This study was undertaken as part of Australian Mineral Industry Research Association (AMIRA) project P511—"Hydrothermal systems, giant ore deposits and a new paradigm for predictive mineral exploration"—while PH was supported by a Natural Sciences and Engineering Research Council of Canada postdoctoral fellowship. The authors gratefully acknowledge logistical support from CODELCO personnel in Chile. Peter Frikken and James Cannell are thanked for assistance with fieldwork while Doug Archibald and Phil Robinson are thanked for analytical assistance. John Walshe is thanked for numerous stimulating discussions. C. Stern and G. Yañez are thanked for incisive reviews and M. Hannington for his editorial handling of this manuscript.

August 4, 2004; July 15, 2005

REFERENCES

Allmendinger, R.W., Figueroa, D., Snyder, D., Beer, J., Mpodozis, C., and Isacks, B., 1990, Foreland shortening and crustal balancing in the Andes at 30 degrees S latitude: Tectonics, v. 9, p. 789–809.

Baksi, A.K., Archibald, D.A., and Farrar, E., 1996, Intercalibration of $^{40}Ar/^{39}Ar$ dating standards: Chemical Geology, v. 129, p. 307–324.

Beccar, L., Vergara, M., and Munizaga, F., 1986, Edades K/Ar de la Formación Farellones en el Cordón del Cerro La Parva, Cordillera de los Andes de Santiago, Chile: Revista Geológica de Chile, v. 28–29, p. 109–113.

Bertens, A., Deckart, K., and Gonzalez, A., 2003, Geocronología U-Pb, Re-Os y ^{40}Ar-^{39}Ar del pórfido de Cu-Mo Los Pelambres, Chile Central [abs.]: Congreso Geologico Chileno, 10th, 2003, Universidad de Concepción, Departamento de Ciencias de la Tierra, Abstracts, p. 40.

Bissig, T., 2001, Metallogenesis of the Miocene El Indio-Pascua gold-silver-copper belt, Chile/Argentina: Geodynamic, geomorphological and petrochemical controls on epithermal mineralization: Unpublished Ph.D. thesis, Kingston, Ontario, Queen's University, 208 p.

Bissig, T., Lee, J., Clark, A., and Heather, K., 2001, The Neogene history of volcanism and hydrothermal alteration in the central Andean flat-slab: New ^{40}Ar-^{39}Ar constraints from the El Indio-Pascua Au (Ag, Cu) belt, III/IV Region, Chile, Provincia San Juan, Argentina: International Geology Reviews, v. 43, p. 312–340.

Bissig, T., Clark, A., and Lee, J., 2002, Miocene landscape evolution and geomorphologic controls on epithermal processes in the El Indio-Pascua Au-Ag-Cu belt, Chile and Argentina: ECONOMIC GEOLOGY, v. 97, p. 971–996.

Bissig, T., Clark, A., Lee, J., and von Quadt, A., 2003, Petrogenetic and metallogenic responses to Miocene slab flattening: Constraints from the El Indio-Pascua Au-Ag-Cu belt, Chile/Argentina: Mineralium Deposita, v. 38, p. 844–862.

Cahill, T., and Isacks, B., 1992, Seismicity and shape of the subducted Nazca plate: Journal of Geophysical Research, v. 97, p. 17503–17529.

Cande, S., and Leslie, R., 1986, Late Cenozoic tectonics of the southern Chile trench: Journal of Geophysical Research, v. 91, p. 471–496.

Cannell, J., Cooke, D.R., Stein, H.J., and Markey, R.J., 2003, New paragenetically constrained Re-Os molybdenite ages for El Teniente Cu-Mo porphyry deposit, central Chile, *in* Eliopoulos, D., Allan, C., Baker, T., Barriga, F., Beaudoin, G., Benardos, A., et al., eds., Mineral exploration and sustainable development: Rotterdam, Millpress, v. 1, p. 255–258.

Charrier, R., Baeza, O., Elgueta, S., Flynn, J., Gans, P., Kay, S., Munoz, N., Wyss, A., and Zurita, E., 2002, Evidence for Cenozoic extensional basin development and tectonic inversion south of the flat-slab segment, southern Central Andes, Chile (33°-36° S.L.): Journal of South American Earth Sciences, v. 15, p. 117–139.

Cooke, D.R., Walshe, J., and Hollings, P., 2005. Giant porphyry copper deposits: Characteristics, distribution, and tectonic controls: ECONOMIC GEOLOGY,v. 100, p. 801–818.

Cuadra, P., 1986, Geochronología K-Ar del yacimiento El Teniente y areas adyacentes: Revista Geológica de Chile, v. 27, p. 16–18.

Dalrymple, G.B., Alexander, E.C., Jr., Lanphere, M.A., and Kraker, G.P., 1981, Irradiation of samples for $^{40}Ar/^{39}Ar$ dating using the Geological Survey TRIGA Reactor: U.S. Geological Survey, Professional Paper 1176, 55 p.

Davidson, P., Kamenetsky, V.S., Cooke, D.R., Frikken, P., Hollings, P., Ryan, C., Van Achterbergh, E., Mernagh, T., Skarmeta, J., Serrano, L., and Vargas R., 2005, Magmatic precursors of hydrothermal fluids at the Río Blanco Cu-Mo deposit, Chile: Links to silicate magmas and metal transport: ECONOMIC GEOLOGY, v. 100, p. 963–978.

Deckart, K., Clark, A.H., Aquilar A, C., and Vargas R, R, 2005, Magmatic and hydrothermal chronology of the giant Rio Blanco porphyry copper deposit, central Chile: Implications of an integrated U-Pb and ^{40}Ar-^{39}Ar database: ECONOMIC GEOLOGY,v. 100, p. 905–934.

Defant, M.J., and Drummond, M.S., 1990, Derivation of some modern arc magmas by melting of young subducted lithosphere: Nature, v. 347, p. 662–665.

Dominguez, S., Malavieille J., and Lallemand S., 2000, Deformation of accretionary wedges in response to seamount subduction: Tectonics, v. 19, p. 182–196.

Godoy, E., 1993, Geologia del area entre los rios Claro del Maipo y Cachapoal: Informe Final del Proyecto Codelco-Servicio Nacional de Geologia y Mineria, v. 1, Texto y Mapas, 68 p.

Godoy, E. and Lara, L., 1994. Segmentacion estructural Andina a los 33°–34°; nuevos datos en la Cordillera principal [Structural Andean segmentation at 33°–34° latitude south; new data on the main Cordillera]: Congreso Geologico Chileno, Antofagasta, Chile, Universidad del Norte Chile, Departamento de Geociencias, Facultad de Ciencias, v. 7, Actas, v. 2, p. 1344–1348.

Godoy, E., Yañez, G., and Vera, E., 1999, Inversion of an Oligocene volcanotectonic basin and uplifting of its superimposed Miocene magmatic arc in the Chilean Central Andes: First seismic and gravity evidences: Tectonophysics, v. 306, p. 217–236.

Hall, C.M., 1981, The application of K-Ar and $^{40}Ar/^{39}Ar$ methods to the dating of recent volcanics and the Laschamp event: Unpublished Ph.D. thesis, Toronto, Canada, University of Toronto, 186 p.

Harris, A.C., Golding, S.D., and White, N.C., 2005, Bajo de la Alumbrera Cu-Au: Stable isotope evidence for a porphyry-related hydrothermal system dominated by magmatic aqueous fluids: ECONOMIC GEOLOGY, v. 100, p. 863–886.

Hildreth, W., and Moorbath, S., 1988, Crustal contributions to arc magmatism in the Andes of central Chile: Contributions to Mineralogy and Petrology, v. 98, p. 455–498.

Kay, S.M., and Abruzzi, J.M., 1996, Magmatic evidence for Neogene lithospheric evolution of the central Andean "flat-slab" between 30° and 32° S: Tectonophysics, v. 259, p. 15–28.

Kay, S., and Mpodozis, C., 2001, Central Andean ore deposits linked to evolving shallow subduction systems and thickening crust: GSA Today, v. 11, p. 4–9.

——2002, Magmatism as a probe to the Neogene shallowing of the Nazca plate beneath the modern Chilean flat-slab: Journal of South American Earth Sciences, v. 15, p. 39–57.

Kay, S.M., Mpodozis, C., Ramos, V., and Munizaga, F., 1991, Magma source variations for mid-late Tertiary magmatic rocks associated with a shallowing subduction zone and a thickening crust in the central Andes (28–33° S): Geological Society of America Special Paper 265, p. 113–137.

Kay, S., Mpodozis, C., Tittler, A., and Cornejo, P., 1994, Tertiary magmatic evolution of the Maricunga mineral belt in Chile: International Geology Reviews, v. 36, p. 1079–1112.

Kay, S.M., Mpodozis, C., and Coira, B., 1999, Neogene magmatism, tectonism and mineral deposits of the central Andes: Society of Economic Geologists Special Publication 7, p. 27–59.

Kay, S.M., Godoy, E. and Kurtz, A., 2005, Episodic arc migration, crustal thickening, subduction erosion, and magmatism in the south-central Andes: Geological Society of America Bulletin, v. 117, p. 67–88.

Kurtz, A.C., Kay, S.M., Charrier, R., and Farrar, E., 1997, Geochronology of Miocene plutons and exhumation history of the El Teniente region, central Chile (34–35°S): Revista Geológica de Chile, v. 24, p. 75–90.

Maksaev, V., Munizaga, F., McWilliams, M., Fanning, M., Mathur, R., Ruiz, J., and Thiele, K., 2002, El Teniente porphyry copper deposit in the Chilean Andes: New geochronological time frame and duration of hydrothermal activity [abs.]: Geological Society of America Abstracts with Programs, v. 34, p. 336.

Martin, M., Clavero, J., Mpodozis, C., and Cutiño, L., 1995, Estudio geológico regional de la franja El Indio, Cordillera de Coquimbo: Servicio Nacional de Geologia y Mineria, Chile, and Compañia Minera San José, Informe registrado IR-95–6, 232 p.

Mathur, R., Ruiz, J.R., and Munizaga, F.M., 2001, Insights into Andean metallogenesis from the perspective of Re-Os analyses of sulphides: Servicio Nacional de Geologia y Mineria, South American Symposium, on Isotope Geology, 3rd, 21–24 October, Pucon, Chile, Universidad de Chile, 2001, 4 p.

Munizaga, F., Maksaev, M., Mathur, R., Ruiz., J., McWilliams, M., and Thiele, K., 2002, Understanding molybdenite Re-Os ages from the El Teniente porphyry copper deposit, Chile [abs.]: Geological Society of America Abstracts with Programs, v. 34, p. 336–337.

Nyström, J.O., Parada, M.A., and Vergara, M., 1993, Sr-Nd isotope compositions of Cretaceous to Miocene volcanic rocks in central Chile: A trend towards MORB signature and a reversal with time: Oxford, London, Symposium on Andean Geodynamics 2, p. 411–414.

Nyström, J.O., Vergara, M., Morata, D., and Levi, B., 2003, Tertiary volcanism during extension in the Andean foothills of central Chile (33°15'-33°45' S): Geological Society of America Bulletin, v. 115, p. 1523–1537.

Onstott, T.C., and Peacock, M.W., 1987, Argon retentivity of hornblendes: A field experiment in a slowly cooled metamorphic terrane: Geochimica et Cosmochimica Acta, v. 51, p. 2891–2904.

Quirt, S., Clark, A. H., Farrar, E., and Sillitoe, R. H., 1971, Potassium-argon ages of porphyry copper deposits in northern and central Chile [abs.]: Geological Society of America Abstracts with Programs, v. 3, p. 676–677.

Reich, M., Parada, M.A., Palacios, C., Dietrich, A., Schultz, F., and Lehmann, B., 2003, Adakite-like signature of late Miocene intrusions at the Los Pelambres giant porphyry copper deposit in the Andes of Central Chile: Metallogenic implications: Mineralium Deposita, v. 38, p. 876–885.

Rivano, S., 1995, Notes for Carta de Geologica de Chile, Hojas Quillota y Portillo, V Region: Servicio Nacional de Geologia de Chile, Carta geologica de Chile Report 73, 202 p.

Rivano, S., and Sepulveda, P., 1986, Hoja Illapel, Illapel sheet, Servicio Nacional de Geologia y Mineria, Carta Geologica de Chile, no. 69, scale 1:250,000.

Rivano, S., Sepulveda, S., Boric, R., and Espineira, D., 1993, Carta de Geologica de Chile, Hojas Quillota y Portillo, V Region: Servicio Nacional de Geologia de Chile, no. 73, scale 1:250,000.

Roddick, J.C., 1983, High precision intercalibration of $^{40}Ar/^{39}Ar$ standards: Geochimica et Cosmochimica Acta, v. 47, p. 887–898.

Sasso, A., and Clark, A., 1998, The Farallón Negro Group, northwest Argentina: Magmatic, hydrothermal and tectonic evolution and implications for Cu-Au metallogeny in the Andean back-arc: Society of Economic Geologists Newsletter 34, p. 1, 8–18.

Serrano, L., Vargas, R., Stambuk, V., Aguilar, C., Galeb, M., Holmgren, C., Contreras, A., Godoy, S., Vela, I., Skewes, M.A., and Stern, C.R., 1996, The late Miocene to early Pliocene Río Blanco-Los Bronces copper deposit, central Chilean Andes: Society of Economic Geologists Special Publication 5, p. 119–130.

Sillitoe, R.H., 1988, Epochs of intrusion-related copper mineralisation in the Andes: Journal of South American Earth Sciences, v. 1, p. 89–108.

Skewes, A., 1992, Miocene and Pliocene copper-rich breccias from the Andes of central Chile (32°-34°S): Unpublished Ph.D. Thesis, Boulder, CO, University of Colorado, 216 p.

Skewes, M.A., and Holmgren, C., 1993, Solevantamiento andino, erosión y emplazamiento de brechas mineralizadas en el deposito de cobre porfídico Los Bronces, chile central (33ºS): Aplicación de geothermometria de inclusiones fluidas: Revista Geológica de Chile, v. 20, p. 71–83.

Skewes, A., and Stern, C.R., 1994, Tectonic trigger for the formation of late Miocene Cu-rich breccia pipes in the Andes of central Chile: Geology, v. 22, p. 551–554.

——1995, Genesis of the giant late Miocene to Pliocene copper deposits of central Chile in the context of Andean magmatic and tectonic evolution: International Geology Review, v. 37, p. 893–909.

——1996, Late Miocene mineralized breccias in the Andes of central Chile: Sr and Nd isotopic evidence for multiple magmatic sources: Society of Economic Geologists Special Publication 5, p. 33–42.

Steiger, R.H., and Jaeger, E., 1977, Subcommission on geochronology: Convention on the use of decay constants in geo- and cosmochronology: Earth and Planetary Science Letters, v. 36, p. 359–362.

Stern, C., 1989, Pliocene to present migration of the volcanic front, Andean Southern Volcanic zone: Revista de Geológica de Chile, v. 16, p. 145–162.

——1991, Role of subduction erosion in the generation of Andean magmas: Geology, v. 19, p. 78–81.

——2001, The subduction erosion of and mantle source evolution of Andean arc magmatism: Isotopic evidence from igneous rocks of central Chile [ext. abs.]: Simposio Sudamericano de Geología Isotópica, 3rd, Pucón, Chile, Extended Abstracts, p. 348–351.

Stern, C.R. and Skewes, M.A., 1995, Miocene to Present magmatic evolution at the northern end of the Andean Southern Volcanic zone, central Chile: Revista Geologica de Chile, v. 22, p. 261–272.

Sun, S.-S., and McDonough, W.F., 1989, Chemical and isotopic systematics of oceanic basalts: Implications for mantle composition and processes Geological Society of London Special Publication 42, p. 313–345.

Thiele, R., 1979, Geologia de la Hoja Santiago, region metropolitana: Instituto de Investigaciones Geologicas, Carta Geologia de Chile, 39, 51 p.

Toro, J.C., 1986, Cuerpos subvolcanicos asociados a zonas de alteracion hidrothermal en la alta cordillera de Chile central: Unpublished Memoria de Titulo, Departamento de Geosciencias, Antofagasta, Universidad del Norte, 174 p.

Vergara, M., Charrier, R., Munizaga, A., Rivano, S., Sepulveda, P., Thiele, R., and Drake, R., 1988, Miocene volcanism in the central Chilean Andes (31°30' S – 34°35' S): Journal of South American Earth Sciences, v. 1, p. 199–209.

Von Huene, R., Corvalán, J., Flueh, E., Hinz, K., Korstgard, J., Ranero, C., Weinrebe, W., and CONDOR Scientists, 1997, Tectonic control of the subducting Juan Fernández Ridge on the Andean margin near Valparaiso, Chile: Tectonics, v. 16, p. 474–488.

Warnaars, F.W., Holmgren, C., and Barassi, S., 1985, Porphyry copper and tourmaline breccias at Los Bronces-Río Blanco, Chile: Economic Geology, v. 80, p. 1544–1565.

Yáñez, G., Ranero, G., von Huene, R., and Diaz, J., 2001, Magnetic anomaly interpretation across a segment of the southern central Andes (32°-34°S): Implications on the role of the Juan Fernández Ridge in the tectonic evolution of the margin during the upper tertiary: Journal of Geophysical Research, v. 106, p. 6325–6345.

Yáñez, G., Cembrano, J., Pardo, M., Ranero, C., and Selles, D., 2002, The Challenger-Juan Fernández-Maipo major tectonic transition of the Nazca-Andean subduction system at 33–34°S: Geodynamic evidence and implications: Journal of South American Earth Sciences, v. 15, p. 23–38.

York, D., 1969, Least squares fitting of a straight line with correlated errors: Earth and Planetary Science Letters, v. 5, p. 320–324.

Yu, Z., Robinson P., and McGoldrick P., 2001, An evaluation of methods for the chemical decomposition of geological materials for trace element determination using ICP-MS: Geostandards Newsletter: Journal of Geostandards and Geoanalysis, v. 25, p. 199–217.

APPENDIX

^{40}Ar-^{39}Ar Analytical Data for Plagioclase and Hornblende Incremental Step-Heating

Laser power	Isotope volumes					Isotope ratios							
(watts)	^{40}Ar	^{39}Ar	^{38}Ar	^{37}Ar	^{36}Ar	$^{40}Ar/^{39}Ar$	$^{38}Ar/^{39}Ar$	$^{37}Ar/^{39}Ar$	$^{36}Ar/^{39}Ar$	Ca/K	$\%^{40}Ar$ atm	f ^{39}Ar	Age
CE-44 plagioclase. J value = 0.002175±0.000009. Plateau date 10.94±0.78 Ma, 85.53% $^{39}Ar/K$													
1 0.75	7.385±0.021	0.610±0.005	0.050±0.003	2.206±0.029	0.028±0.000	12.106±0.009	0.082±0.063	3.617±0.016	0.046±0.077	9.913	92.38	14.47	3.7±4.4
2 1.50	10.395±0.023	1.096±0.008	0.050±0.003	3.603±0.047	0.033±0.000	9.487±0.007	0.046±0.069	3.289±0.015	0.030±0.068	8.852	72.33	26.47	10.6±2.5
3 2.25	6.560±0.012	0.564±0.006	0.039±0.003	1.685±0.022	0.023±0.000	11.622±0.010	0.069±0.078	2.984±0.016	0.042±0.098	8.308	78.32	13.15	10.5±5.1
4 3.50	6.800±0.015	0.768±0.006	0.055±0.003	1.212±0.017	0.022±0.000	8.851±0.008	0.072±0.060	1.577±0.016	0.028±0.100	4.268	69.48	18.37	10.9±3.5
5 7.00	9.989± 0.017	1.130±0.007	0.102±0.004	3.849±0.050	0.030±0.000	8.840±0.007	0.090±0.040	3.407±0.015	0.026±0.082	9.106	67.39	27.53	11.5±2.6
Total or average	40.566±0.040	3.942±0.015	0.240±0.008	17.521±0.079	0.108±0.005	10.292±0.002	0.061±0.016	4.445±0.003	0.027±0.023	8.160		100.00	9.9±0.7
CE-21 plagioclase. J value = 0.002177±0.000009. Plateau date 12.38±0.86 Ma, 79.01% $^{39}Ar/K$													
1 0.75	8.956±0.032	0.756±0.007	0.073±0.004	1.675±0.042	0.033±0.000	11.843±0.009	0.096±0.060	2.215±0.027	0.044±0.069	6.000	89.72	20.99	4.9±3.7
2 1.50	9.958±0.016	1.167±0.008	0.049±0.003	2.045±0.027	0.029±0.000	8.536±0.007	0.042±0.065	1.753±0.015	0.024±0.080	4.723	62.36	32.54	13.0±2.4
3 2.25	5.694±0.015	0.772±0.006	0.039±0.003	1.031±0.014	0.017±0.000	7.375±0.009	0.051±0.069	1.336±0.016	0.022±0.134	3.632	57.39	21.26	12.8±3.6
4 7.00	10.624±0.018	0.904±0.007	0.137±0.005	3.187±0.041	0.034±0.000	11.756±0.008	0.152±0.036	3.527±0.015	0.038±0.069	9.548	76.36	25.21	11.3±3.2
Total or average	34.761±0.043	3.401±0.014	0.249±0.008	11.075±0.066	0.089±0.005	10.221±0.002	0.073±0.016	3.257±0.004	0.026±0.026	5.973		100.00	10.8±0.8
CN-46 plagioclase. J value = 0.002163±0.000013. Plateau date 15.41±0.45 Ma, 78.60% $^{39}Ar/K$													
1 0.50	5.298±0.013	0.149±0.003	0.047±0.004	0.190±0.004	0.019±0.000	35.642±0.018	0.316±0.077	1.276±0.026	0.127±0.090	3.520	89.78	1.78	15.3±14.1
2 1.00	17.849±0.122	1.517±0.134	0.163±0.033	1.842±0.024	0.056±0.000	11.764±0.089	0.108±0.220	1.214±0.089	0.037±0.097	3.141	84.64	19.62	7.0±1.8
3 1.50	5.445±0.016	0.557±0.005	0.033±0.003	0.711±0.010	0.017±0.000	9.775±0.009	0.059±0.095	1.276±0.016	0.030±0.106	3.452	63.40	6.83	14.6±3.9
4 2.25	30.921±0.037	2.696±0.014	0.097±0.005	3.685±0.047	0.077±0.000	11.469±0.005	0.036±0.049	1.367±0.014	0.028±0.030	3.541	66.26	34.82	15.2±1.0
5 2.75	9.349±0.015	0.766±0.006	0.046±0.004	0.964±0.013	0.027±0.000	12.211±0.008	0.060±0.090	1.260±0.016	0.035±0.063	3.336	68.05	9.63	15.6±2.6
6 3.50	8.326±0.018	0.655±0.005	0.054±0.004	0.987±0.014	0.024±0.000	12.720±0.008	0.082±0.073	1.507±0.016	0.037±0.074	3.990	68.98	8.25	15.8±3.3
7 5.00	9.966±0.016	0.881±0.006	0.080±0.004	1.793±0.024	0.027±0.000	11.313±0.007	0.091±0.049	2.035±0.015	0.031±0.068	5.351	65.92	11.22	15.3±2.5
8 7.00	7.881±0.015	0.622±0.005	0.061±0.003	3.968±0.051	0.024±0.000	12.679±0.008	0.099±0.054	6.384±0.015	0.038±0.071	17.012	67.18	7.86	16.7±3.2
Total or average	94.690±0.133	7.621±0.136	0.521±0.034	19.661±0.080	0.234±0.005	12.425±0.009	0.068±0.034	2.580±0.009	0.031±0.014	4.730		100.00	13.8± 0.4
CN-18 plagioclase. J value = 0.002170±0.000010. Plateau date 10.11±2.37 Ma, 41.46% $^{39}Ar/K$													
1 0.50	28.137±0.033	0.833±0.006	0.657±0.009	1.376±0.018	0.101±0.000	33.794±0.007	0.790±0.015	1.653±0.015	0.121±0.026	4.370	98.31	35.32	2.2±3.8
2 1.00	10.404±0.032	0.444±0.004	0.239±0.006	0.678±0.010	0.041±0.000	23.443±0.011	0.538±0.026	1.527±0.018	0.092±0.049	4.161	99.74	18.16	0.1±5.5
3 1.5	11.121±0.020	0.397±0.005	0.232±0.007	0.759±0.011	0.042±0.000	28.018±0.012	0.584±0.031	1.913±0.018	0.105±0.047	5.353	93.36	15.81	7.9±6.1
4 2	7.523±0.013	0.271±0.003	0.177±0.005	0.486±0.007	0.029±0.000	27.761±0.013	0.655±0.031	1.793±0.020	0.108±0.060	5.105	92.61	10.58	8.9±8.3
5 2.5	4.811±0.013	0.178±0.004	0.115±0.004	0.293±0.005	0.020±0.000	27.017±0.021	0.645±0.043	1.643±0.027	0.113±0.090	4.849	90.18	6.67	12.0±13.3
6 3.25	4.660±0.015	0.139±0.004	0.087±0.004	0.228±0.004	0.019±0.000	33.507±0.026	0.624±0.048	1.640±0.031	0.139±0.087	4.953	91.08	5.07	13.9±16.0
7 5	4.971±0.014	0.098±0.003	0.048±0.003	0.266±0.005	0.021±0.000	50.698±0.035	0.488±0.074	2.708±0.039	0.210±0.088	8.825	94.00	3.33	15.2±25.2
8 7	3.780±0.012	0.136±0.003	0.081±0.004	0.453±0.007	0.017±0.000	27.714±0.024	0.591±0.050	3.324±0.029	0.125±0.107	10.043	98.52	5.05	1.8±18.0
Total or average	75.004±0.059	2.271±0.011	1.550±0.015	6.269±0.027	0.245±0.005	33.025±0.003	0.682±0.006	2.760±0.003	0.108±0.011	5.061		100.00	5.1±1.4

Appendix *(Cont.)*

Laser power	Isotope volumes					Isotope ratios							
(watts)	^{40}Ar	^{39}Ar	^{38}Ar	^{37}Ar	^{36}Ar	^{40}Ar/^{39}Ar	^{38}Ar/^{39}Ar	^{37}Ar/^{39}Ar	^{36}Ar/^{39}Ar	Ca/K	%^{40}Ar atm	f ^{39}Ar	Age
CN-45 hornblende. J value = 0.002178±0.000009. Plateau date 11.62±0.72 Ma, 90.02% ^{39}Ar/K													
1	3.193±0.020	0.246±0.005	0.060±0.005	0.372±0.006	0.021±0.000	12.989±0.022	0.244±0.089	1.512±0.027	0.085±0.102	5.13	149.81	9.98	-32.53±13.51
2	7.483±0.017	1.746±0.010	0.364±0.008	11.825±0.150	0.020±0.000	4.285±0.006	0.208±0.022	6.772±0.014	0.011±0.104	18.686	32.12	90.02	11.62±1.45
Total or average	10.305±0.026	1.847±0.011	0.384±0.009	17.371±0.151	0.028±0.003	5.580±0.003	0.208±0.012	9.406±0.005	0.015±0.053	17.328		100	7.24± 0.93
CN-37 hornblende. J value = 0.002176±0.000009. Plateau date 21.90±1.28 Ma, 59.58% ^{39}Ar/K													
1	2.105±0.027	0.320±0.006	0.056±0.005	0.172±0.004	0.016±0.000	6.578±0.024	0.174±0.098	0.537±0.031	0.051±0.127	1.615	175.15	16.68	-22.0± 9.1
2	1.170±0.012	0.252±0.005	0.033±0.003	0.089±0.003	0.009±0.000	4.634±0.022	0.131±0.097	0.353±0.037	0.037±0.213	1.106	78.39	11.33	4.5±12.8
3	1.336±0.010	0.259±0.005	0.069±0.004	1.547±0.021	0.008±0.000	5.149±0.021	0.268±0.064	5.963±0.024	0.030±0.230	20.63	43.07	12.41	13.2±10.7
4	5.831±0.016	1.006±0.007	0.273±0.007	9.619±0.123	0.011±0.000	5.797±0.008	0.271±0.026	9.562±0.015	0.011±0.188	26.946	7.18	59.58	21.9±2.5
Total or average	9.732±0.035	1.578±0.012	0.363±0.010	16.235±0.125	0.022±0.004	6.166±0.004	0.230±0.014	10.286±0.005	0.014±0.091	18.961		100	11.5± 1.5

Notes: Measured volumes are 1E-10cm^3; all ages are Ma and errors are 2σ;. %^{40}Ar atm = percentage of atmospheric ^{40}Ar; f ^{39}Ar =fraction of ^{39}Ar; isotope production ratios: (^{40}Ar/^{39}Ar)K = 0.0302, (^{37}Ar/^{39}Ar)Ca = 1416.4306, $(^{36}Ar/^{39}Ar)_{Ca}$ = 0.3952, Ca/K = 1.83 × $(^{37}Ar_{Ca}/^{39}Ar_{K})$